Astron. Astrophys. 339, 355–381 (1998)

ASTRONOMY AND ASTROPHYSICS

A new scenario of galaxy evolution under a universal Initial Mass Function

C. Chiosi[1,2], **A. Bressan**[3], **L. Portinari**[2], **and R. Tantalo**[2]

[1] European Southern Observatory, Karl-Schwarzschild-Strasse 2, D-85748 Garching bei München, Germany
[2] Department of Astronomy, University of Padova, Vicolo dell'Osservatorio 5, I-35122 Padova, Italy
[3] Astronomical Observatory, Vicolo dell'Osservatorio 5, I-35122 Padova, Italy

Received 7 August 1997 / Accepted 16 July 1998

Abstract. In this paper, basic observational properties of elliptical galaxies such as the integrated spectra, the chemical abundances and the enhancement of α-elements inferred from broad-band colors and line strength indices Mg_2 and $\langle\mathrm{Fe}\rangle$ (and their gradients), the color-magnitude relation, the UV fluxes, and the mass-luminosity ratios, are examined in the light of current theoretical interpretations, and attention is called on several points of internal contradiction. Indeed existing models for the formation and evolution of elliptical galaxies are not able to simultaneously account for all of the above observational features. Specifically, in the context of standard star formation in the galactic-wind driven models, that are at the base of present-day understanding of the color-magnitude relation and UV fluxes, it is difficult to explain the slope of the M/L_B versus M_B relation (tilt of the Fundamental Plane) and enhancement of the α-elements in the brightest elliptical galaxies. We suggest that the new initial mass function (IMF) by Padoan et al. (1997), which depends on the temperature, density, and velocity dispersion of the medium in which stars are formed, may alleviate some of the difficulties in question. Models of elliptical galaxies incorporating the new IMF (varying with time and position inside a galaxy) are presented and discussed at some extent. In brief, in a hot, rarefied medium the new IMF is more skewed toward the high mass end than in a cool, dense medium, a situation which is met passing from high to low mass galaxies or from the external regions to the center of a galaxy. As a result of the changing IMF, the enhancement of α-elements and tilt of the Fundamental Plane are easily explained leaving unaltered the interpretation of the remaining properties under examination. Finally, some implications concerning the relative proportions of visible stars, collapsed remnants (baryonic dark matter), and gas left over by the star forming process are examined.

Key words: stars: luminosity function, mass function – galaxies: elliptical and lenticular, cD – galaxies: evolution – galaxies: formation

1. Introduction

The conventional picture of star formation in elliptical galaxies is one in which the galaxies and their stellar content formed early in the universe and have evolved quiescently ever since. This view is supported by the apparent uniformity of ellipticals in photometric and chemical appearance (cf. Matteucci 1997 for a recent review) and the existence of scaling relations, e.g. the fundamental plane (cf. Bender 1997). In contrast, the close scrutiny of nearby ellipticals makes evident a large variety of morphological and kinematic peculiarities and occurrence of star formation in a recent past (Schweizer et al. 1990, Schweizer & Seitzer 1992, Longhetti et al. 1997a,b). All this leads to a different picture in which elliptical galaxies are formed by mergers and/or accretion of smaller units over a time scale comparable to the Hubble time. Furthermore, strong evolution in the population of early type galaxies has been reported by Kauffmann et al. (1996) which has been considered to support the hierarchical galaxy formation model (Kauffmann et al. 1993, Baugh et al. 1996).

Tracing back the formation mechanism of elliptical galaxies from the bulk of their chemo-spectro-photometric properties is a cumbersome affair because studies of stellar populations in integrated light reveal only luminosity weighted ages and metallicities, and are ultimately unable to distinguish between episodic (perhaps recurrent) and monolithic histories of star formation and between star formation histories in isolation or interaction. In any case, there are a number of primary observational constraints that should be met by any model of galaxy formation and evolution (they will be briefly summarized below). As nowadays most properties of elliptical galaxies have been studied with sophisticated chemo-spectro-photometric models in which the dynamical process of galaxy formation is reduced to assuming either the closed box or infall scheme and a suitable law of star formation (Arimoto & Yoshii 1987, 1989; Bruzual & Charlot 1993; Bressan et al. 1994; Worthey 1994; Einsel et al. 1995; Tantalo et al. 1996; Bressan et al. 1996; Gibson 1996a,b; Gibson 1997; Gibson & Matteucci 1997; Tantalo et al. 1998a, TCBMP98). In contrast, the highly sophisticated dynamical models of galaxy formation (Davis et al. 1992; Navarro & Steinmetz 1997; Haehnelt et al. 1996a,b; Katz 1992; Katz & Gunn 1991; Katz et al. 1996; Steinmetz & Mueller 1995; Navarro et al. 1996; Steinmetz 1996a,b and references), owing to the complexity of the problem, are still somewhat unable to make detailed predictions about the chemo-spectro-photometric

Send offprint requests to: C. Chiosi

properties of the galaxies in question. Attempts to bridge the two aspects of the same problem are by Theis et al. (1992 and references) and most recently Contardo et al. (1998) and Carraro et al. (1998).

However, even in the case of the chemo-spectro-photometric approach, extant models, which ultimately stem from the classical galactic wind driven model of Larson (1974), often come to solutions that are mutually discordant, when trying to explain one or another of the properties of elliptical galaxies.

In this study we would like to propose a coherent scenario in which the effects of using a new IMF are explored. The key idea is to adopt an IMF whose properties change with the physical conditions of the star forming medium, which in turn are related to the mean gas density of galaxies. The study stands on the adoption of the IMF recently proposed by Padoan et al. (1997) which depending on temperature, density and velocity dispersion of the star forming gas may bring a new leverage to the whole problem and yield results perhaps able to improve upon some of the above points of contradiction.

The plan of the paper is as follows. Sect. 2 shortly reviews the basic observational data and their current interpretation. Sect. 3 shortly presents the IMF of Padoan et al. (1997). Sect. 4 describes our prescriptions for models of elliptical galaxies, in which the new IMF is an essential ingredient. Sect. 5 discusses at some extent the heating-cooling balance of the gas that is required to derive temperature, density, and velocity dispersion to be used with the IMF. Sect. 6 introduces the thermal model of the star forming process and how this is coupled with the IMF. Sect. 7 presents the reference models and discusses some of their general properties. Sect. 8 analyzes in detail the model results concerning the history of star formation and chemical enrichment, the fractionary masses of visible and remnant stars, and the variation of the IMF with age and galactic mass. Sect. 9 presents the broad-band colors and magnitudes and the mass to light ratios of the models. In particular, it presents our fits of the color-magnitude relation and fundamental plane. Finally, a summary and some concluding, critical remarks are given in Sect. 10.

2. Learning from observations

2.1. The G-dwarf analog

As first noticed by Bressan et al. (1994, BCF94), the near UV spectrum (2000 Å to 3500 Å) of elliptical galaxies shows that the relative percentage of old metal-poor stars is small, thus indicating that the metallicity partition function $N(Z)$, i.e. number of stars per metallicity bin, cannot be the one predicted by the closed-box scheme. In analogy with the G-dwarf problem in the solar vicinity (cf. Tinsley 1980), whose solution is found in models with infall (Lynden-Bell 1975), Tantalo et al. (1996, TCBF96) show that also in the case of elliptical galaxies the infall scheme removes the above discrepancy. Similar conclusion is reached by Greggio (1996), who however favors the prompt enrichment alternative.

2.2. The chemical abundances

Abundances in elliptical galaxies up to now have been deduced either from integrated colors, spectra, or line-strength indices (Carollo et al. 1993, Carollo & Danziger 1994a,b, Davies et al. 1993; Schombert et al. 1993) together with their spatial gradients. In general what is measured is a complicated result of age and metallicity, so that disentangling age from metallicity effects is the primary task of any study aimed at evaluating the metallicity of these galaxies (cf. the recent review by Matteucci 1997). Metallicity indicators such as Mg_2 and $\langle\mathrm{Fe}\rangle$ are the most used to derive information on metallicity. Although passing from the line strength indices Mg_2 and $\langle\mathrm{Fe}\rangle$ to chemical abundances is not a straight process (cf. Tantalo et al. 1998b, TBC98), arguments are given to conclude that the mean $[\mathrm{Mg/Fe}]$ ratio exceeds that of the most metal-rich stars in the solar vicinity by about 0.2-0.3 dex (enhancement of α-elements; O, Mg, Si, etc.. with respect to Fe), and the ratio $[\mathrm{Mg/Fe}]$ increases with the galactic mass up to this value (cf. Matteucci 1994, 1997). The enhancement of α-elements is particularly demanding as it implies that a unique source of nucleosynthesis has been contributing to chemical enrichment (type II SN from massive stars, the main producers of Mg). It follows from this that in the standard star formation scenario, i.e. with constant IMF, the maximum duration of the star forming activity should decrease when the galaxy mass increases ($\Delta t_{SF} \propto M_G^{-1}$).

2.3. The color-magnitude relation

Elliptical galaxies obey a mean color-magnitude relation (CMR): colors get redder at increasing luminosity, cf. Bower et al. (1992) for galaxies in the Virgo and Coma clusters and Schweizer & Seitzer (1992) for galaxies in small groups and field. The cluster CMR is particularly narrow, whereas the field CMR is more disperse. Long ago Larson (1974) postulated that the present-day CMR is the consequence of SN-driven galactic winds. In the classical scenario, massive galaxies eject their gaseous content much later and get higher mean metallicities than less massive ones. This implies that $\Delta t_{SF} \propto M_G$, contrary to the trend required by the α-enhancement problem. The tightness of the cluster CMR (in the U-V color) suggests that most galaxies are nearly coeval with ages ranging from 13 to 15 Gyr (Bower et al. 1992). The CMR for field galaxies is likely compatible with more recent episodes of star formation, perhaps interactions spread over several Gyrs (Schweizer & Seitzer 1992, Longhetti et al. 1997a,b). The CMR is currently interpreted as a mass-metallicity sequence rather than an age sequence along which bluer galaxies are significantly younger than red galaxies (cf. BCF94, TCBF96, TCBMP98, and Kodama & Arimoto 1996). However, whether the age plays also a role (in particular towards to low luminosity end of the CMR) is not yet clarified.

2.4. The age-metallicity dilemma

The stellar content of a galaxy gets redder both at increasing age and metallicity thus giving rise to the well known age-metallicity

dilemma. The H_β and [MgFe] indices are particularly suited to cast light on their separate effects, because H_β is a measure of the turn-off color and luminosity, and age in turn, whereas [MgFe] is more sensitive to the RGB color and hence metallicity. Analyzing the Gonzáles (1993) data Bressan et al. (1996, BCT96) and Greggio (1996) got the following provisional conclusions: (i) most galaxies seem to possess nearly identical chemical structures, i.e. high mean metallicities and narrow range of metallicities ; (ii) galaxies do not distribute along the locus expected from the CMR of coeval old objects (BCT96). In contrast, they seem to follow a sequence of about constant metallicity and varying age so that recent episodes of star formation (bursts) have been suggested. Looking at the difference in H_β and [MgFe] between the nuclear region (i.e. *Re*/8 : N) and the whole galaxy (i.e. *Re*/2: W), and translating $\Delta H_{\beta NW}$ and $\Delta[MgFe]_{NW}$ into Δt_{NW} and ΔZ_{NW}, i.e. in age and metallicity difference, respectively, BCT96 pointed out that in most galaxies the nucleus is younger and more metal-rich than the external regions, and suggested that $\Delta t_{NW} \simeq \Delta t_{SF} \propto 1/\Sigma \propto 1/M_G$. More recently, Tantalo et al. (1998c, TCB98), applying to the Gonzáles (1993) sample the simultaneous analysis of the indices H_β, Mg_2, and $\langle Fe \rangle$ suggested that in most galaxies the nucleus is younger, more metal-rich and more enhanced in α-elements than the peripheral regions, and limited to smaller subgroup of the same sample that the duration of the star forming activity was short in the bright ellipticals and long in the the less luminous ones. In this context, Kuntschner & Davies (1998), analyzing the line strength indices for a complete sample of early type galaxies (brighter than $M_B = -17$) in the Fornax cluster find that the elliptical are old objects with metallicity varying from roughly solar to three times solar, whereas the lenticular galaxies spread to younger ages indicating a more extended period of star formation. More data and more sophisticated analyses are needed to cast light on the whole subject.

2.5. The ultraviolet excess

All studied elliptical galaxies have detectable UV flux shortward of about 2000 Å (Burstein et al. 1988) with large variations from galaxy to galaxy. The intensity of the UV emission as measured by the (1550-V) color correlates with the Mg_2 index, the central velocity dispersion Σ_c, and the luminosity (mass) of the galaxy. Finally, the HUT observations by Ferguson et al. (1991) and Ferguson & Davidsen (1993) of the UV excess in the bulge of M31, in which a drop-off short-ward of about 1000 Å is detected, indicate that the temperature of the emitting source must be about 25,000 K. Only a small percentage of the $912 \leq \lambda \leq 1200$ Å flux can be coming from stars hotter than 30,000 K and cooler than 20,000 K.

Most likely, the UV excess owes its origin to an old component that gets hot enough to power the ISED of a galaxy in the far UV regions. Several possible candidates are envisaged (cf. Greggio & Renzini 1990, BCF94 and TCBF96). The appearance of the various types of UV sources is governed by several important physical factors, each of which is affected by a certain degree of uncertainty still far from being fully assessed. These are the efficiency of mass loss during the RGB and AGB phases, the enrichment law $\Delta Y/\Delta Z$ and finally, for the specific case of P-AGB stars the detailed relation between the initial and final mass of the stars at the end of the AGB phase. Popular sources of UV radiation are:

(1) the classical post asymptotic giant branch (P-AGB) stars (see Bruzual & Charlot 1993, Charlot & Bruzual 1991), which are always present in the stellar mix of a galaxy. They cannot, however, be the sole source of UV flux because of their high mean temperature (about 100,000 K) and lack of sufficient fuel (cf. Greggio & Renzini 1990). Furthermore, they hardly explain the correlation with Mg_2 and Σ_c.

(2) Very blue HB (VB-HB) stars of extremely low metallicity (Lee 1994). These stars have effective temperatures hotter than about 15,000 K but much cooler than those of the P-AGB stars. Therefore, depending on their actual $T_{\rm eff}$, they can generate ISEDs in agreement with the observational data provided that the age is let vary from galaxy to galaxy (Park & Lee 1997). It must be checked, however, whether the percentage of low metallicity stars is compatible with the G-Dwarf problem above.

(3) The H-HB and AGB-manqué stars of high metallicity (say $Z>0.07$) which are expected to be present albeit in small percentages in the stellar content of bulges and elliptical galaxies in general (Bertelli et al. 1995). Indeed, these stars have effective temperatures in the right interval and generate ISEDs whose intensity drops short-ward of about 1000 Å by the amount indicated by the observational data. With normal mass loss and $\Delta Y/\Delta Z = 2.5$ (Pagel et al. 1992), the first H-HB and AGB manqué stars occurs at the age of about 5.6 Gyr. This age is lowered if $\Delta Y/\Delta Z$ is higher than 2.5.

(4) Finally, the analog of the above H-HB and AGB-manqué stars, but generated by enhancing the mass loss rate during the RGB phase at increasing metallicity. These type of stars have been named by Dorman et al. (1993, 1995) extremely hot HB objects (E-HB). They share nearly the same properties of the H-HB and AGB-manqué stars. The main difficulty with this option is the uncertainty concerning the metallicity dependence of the mass loss rate (cf. Carraro et al. 1996).

The most probable channels, i.e. items (3) and (4) above, require a suitable metallicity partition $N(Z)$, in which high metallicity bins are populated (a few percent of the total are fully adequate), provide a simple explanation for the dependence of the (1550-V) color on Mg_2 (metallicity ?), velocity dispersion Σ_c, and luminosity of the parent galaxy, but in turn pose strong constraints on the past history of star formation and chemical enrichment so that the right $N(Z)$ is generated.

2.6. The iron discrepancy

Elliptical galaxies have extended haloes of gas emitting in the X-ray band. Other indications of the existence of such haloes come from HI kinematics, planetary nebulae, gravitational lensing, and dynamical studies (cf. Carollo et al. 1995 and references). Measurements of the iron content in the X-ray emitting gas (hot inter-stellar medium, H-ISM) from the ASCA data indicate a very low abundance, much lower (some time up a factor of 10)

than the iron content of the stellar populations in these galaxies as derived from integrated optical spectra (Arimoto et al. 1997). Several causes are thoroughly examined by Arimoto et al. (1997) going from supernova enrichment, chemical evolution of galaxies and clusters of galaxies, gas flows, heating of intra-cluster medium to reliability of the diagnostic used to derive iron abundances from X-ray observations. The problem is still unsettled.

2.7. Oxygen over-abundance and iron-luminosity relation of ICM

X-ray observations of the hot intra-cluster medium (ICM) of galaxies by Mushotzsky (1994) show an oxygen overabundance relative to iron of [O/Fe]=0.1 ÷ 0.7. This result is an important constraint to the past chemical history of elliptical galaxies, since thought to be the major contributors to the enrichment of the ICM. In brief, galactic winds are the favored mechanism to eject metal-rich gas (Matteucci & Vettolani 1988) provided that a flatter IMF than the Salpeter case is used to account for the amount of Fe and the [O/Fe] ratio at the same time (David et al 1991; Matteucci & Gibson 1995). Bimodal star formation (Elbaz et al. 1995), while explaining the abundance ratios, seems to be unable to match the CMR (Gibson 1996b). All these models, while recovering the total ICM iron mass, could only account for part of the total mass of gas measured in the X-ray band (Arnaud 1994). Following a suggestion by Trentham (1994) that the precursors of the dwarf galaxies populating the faint end of the luminosity function may in fact be the source for 100% of the ICM gas, Gibson & Matteucci (1997) show that the bulk of the ICM gas cannot originate within the dwarf precursors unless the pre-wind binding energy was 4-5 times lower than the present day values. Finally, the ICM iron mass increases as a function of the cluster optical luminosity (E+S0 galaxies) such that $M_{Fe}^{ICM} \simeq 0.02 L_V$ (Arnaud et al. 1992).

2.8. The fundamental plane

Elliptical galaxies do not populate uniformly the parameter space with central velocity dispersion Σ_c, effective radius R_e, and surface brightness I_e as coordinates. They cluster around a plane called the *Fundamental Plane*. Using the coordinate system defined by Bender et al. (1992) and the identities

$$L = c_1 I_e R_e^2 \tag{1}$$

$$M = c_2 \Sigma_c^2 R_e \tag{2}$$

with c_1 and c_2, suitable constants, the physical coordinates are translated into

$$k_1 = \frac{1}{\sqrt{2}} log[\frac{M}{c_2}] \tag{3}$$

$$k_2 = \frac{1}{\sqrt{6}} log[\frac{c_1}{c_2}(\frac{M}{L}) I e^3] \tag{4}$$

$$k_3 = \frac{1}{\sqrt{3}} log[\frac{c_1}{c_2}(\frac{M}{L})]. \tag{5}$$

Of particular relevance is the projection of the FP onto the $k_1 - k_3$ plane, where the FP is seen edge on. Limited to the case of the Virgo elliptical galaxies to avoid distance uncertainties, the relation $k_3 = 0.15 k_1 + 0.36$ with $\sigma(k_3) = 0.05$ is found to hold (cf. Ciotti et al. 1996 for details). The ratio (M/L) increases with galaxy mass (tilt of the FP).

Unfortunately, current models of elliptical galaxies that fairly match other key properties of these systems are still unable to account for the tilt of the FP. Specifically, under standard assumptions for the IMF and star formation rate, at any given age the models predict M/L_B ratios that are nearly constant at increasing luminosity (mass) of the galaxy, and that increase with the age at fixed galactic mass. See for instance the M/L_B versus L_B relations of the BCT96 and TCBF96 models. An easy way out of the problem would be that low mass galaxies are truly young objects (in the sense that dominant star formation started much later than in less massive ones). For the arguments discussed above, this alternative seems to be unlikely.

Renzini & Ciotti (1993) investigated two possible origins of the tilt: a systematic variation of the IMF (of power-law type) and a trend in the relative proportions and distributions of bright and dark matter. The conclusion is that in both cases, in order to explain the tilt and tightness of the FP at the same time, major changes and fine tuning are required. In brief, the IMF or relative bright/dark matter distribution should change along the FP, but at every position a small dispersion in the IMF or relative bright/dark matter distribution are required to preserve the tightness. In a subsequent paper along the same vein, Ciotti et al. (1996) looked at various effects of structural and dynamical nature (such as orbital radial anisotropy, relative bright/dark matter distributions, shape of the light profiles) under the assumption of a constant stellar mass to light ratio. While anisotropy gives a marginal effect, variations in the bright/dark matter distributions and/or shape of the light profiles can produce the tilt. Also in this case fine tuning is however required to preserve the tightness of the FP.

2.9. How to reconcile things ?

It is evident that up to now no coherent explanation is available for the pattern of properties of elliptical galaxies. Most striking is that, while the gradients in H_β and $[\mathrm{MgFe}]$ and trend for the ratio $[\mathrm{Mg/Fe}]$ with galaxy mass (Davies et al. 1993; Matteucci 1994) suggest that the duration of the star formation activity ought to be shorter in massive galaxies than in low mass ones, the opposite should occur to account for the slope of the CMR.

In the contest of conventional picture of star formation in elliptical galaxies (formation and evolution in isolation), we address the question whether relaxing some of the standard assumptions a viable solution can be found. As already recalled, among the various suggestions advanced to explain the FP tilt, Renzini & Ciotti (1993) explored the effect of varying the IMF and concluded that major but suitable change of the IMF are required.

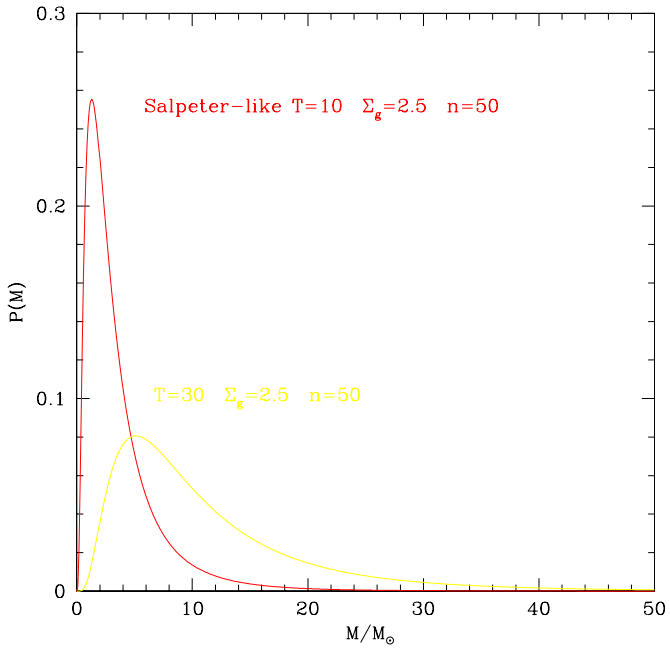

Fig. 1. The IMF of Padoan et al. (1997) for two different values of the temperature (10 and 30 K) and constant density ($n = 50\ cm^{-1}$) and velocity dispersion $\Sigma_g = 2.5\ km\ s^{-1}$. Similar curves are possible at varying density and velocity dispersion. Note how the IMF may change from a Salpeter-like law (very small M_P) to cases very different from the classical behavior.

3. A universal IMF

Padoan et al. (1997) have proposed a new IMF which depends on the the physical conditions of the star forming medium, i.e. temperature, density and velocity dispersion. This IMF stems from a statistical description of the density field emerging from randomly forced supersonic flows in star forming regions. Hydrodynamical simulations of supersonic flows indicate that very large density contrasts can develop with log-normal probability distribution.

Although the physical foundations of the Padoan et al. (1997) IMF have been questioned by Scalo et al. (1997), thus weakening the adoption of this particular IMF, we think it wise to explore in a systematic a fashion the potential of an IMF whose properties change with the physical conditions of the medium (and likely galaxy type).

The Padoan et al. (1997) IMF is

$$\int_0^\infty \phi(M)dM =$$

$$\int_0^\infty \frac{2B^2}{(2\pi\sigma^2)^{0.5}} M^{-3} exp[-0.5(\frac{2lnM - A}{\sigma})^2]dM = 1. \quad (6)$$

The quantities A, B and σ are defined by the following relations:

$$A = 2\ln B + 0.5\sigma^2, \quad (7)$$

$$B = 1.2 \times (T/10)^{1.5} \times (n/1000)^{-0.5}, \quad (8)$$

$$\sigma^2 = \ln[1 + 0.36(\mathcal{M}^2 - 1)], \quad (9)$$

in which σ is the standard deviation of the number density distribution in the field with respect to the mean. $\mathcal{M}$ is the Mach number given by $\mathcal{M}^2 = (\Sigma_g/v_s)^2$, T is the temperature in K, n is the number density in cm^{-3}, v_s is the sound velocity, and Σ_g (in km/s) is the velocity dispersion of the star forming gas. This IMF has a long tail at high masses, an exponential cutoff at the smallest masses, a characteristic peak mass

$$M_P \simeq 0.2M_\odot \times (T/10)^2 \times (n/1000)^{-0.5} \times (\Sigma_g/2.5)^{-1}, \quad (10)$$

and a slope continuously varying with the mass. The IMF gets flatter and M_P gets higher at increasing temperature or decreasing density and velocity dispersion. The opposite occurs reversing the variations of the three physical parameters. The response of the IMF to variations in temperature is shown in Fig. 1 for values of density and velocity dispersion Σ_g typical of molecular clouds, i.e. $n = 50$ particles per cm^3, and $\Sigma_g = 2.5$ km s^{-1}. See Padoan et al. (1997) for all other details.

The IMF is analytically integrable. Performing the change of variable $M = e^t$ and writing

$$\alpha = \frac{2B^2}{(2\pi)^{0.5}\sigma}; \qquad \beta = 2; \qquad \gamma = \frac{2}{\sigma^2}; \qquad \delta = \frac{A}{2}$$

one gets

$$\int_o^\infty \phi(M)dM = \int_{-\infty}^\infty \alpha e^{-\beta t} e^{-[-\gamma(t-\delta)^2]}dt \quad (11)$$

whose general solution is

$$\int_{-\infty}^{t^*} \phi(t)dt = 0.5[1. + Erf(x)] \quad (12)$$

with

$$x = \frac{\beta - 2\gamma\delta + 2\gamma t^*}{2(\gamma)^{0.5}} \quad (13)$$

and

$$Erf(x) = \frac{2}{\sqrt{\pi}} \int_0^x exp(-z^2)dz. \quad (14)$$

4. Modelling elliptical galaxies

The new IMF has been implemented in a simplified version of the TCBMP98 models of elliptical galaxies in which spatial gradients of mass density (baryons and dark matter) and star formation are taken into account. For the sake of simplicity and better understanding of the role played by the sole IMF, we adopt here the closed-box formulation (no infall of primordial gas).

4.1. Sketch of the models

Elliptical galaxies are modelled as a spherical distribution of baryonic material with total mass $M_{L,T}$ (originally in form of gas) embedded in a large halo of dark matter with total mass $M_{D,T}$. Both components have suitable radial distributions. For the purposes of this study, we will limit ourselves to consider only the region of the galaxy inside the effective radius R_e, treated as single density-averaged zone. As far as dark matter is concerned this is included assuming that the ratios of dark to luminous mass and radius are $M_{D,T}/M_{L,T} = \zeta = 5$ and $R_D/R_L = \zeta = 5$ (cf. Bertin et al. 1992; Saglia et al. 1992). Other values of ζ are possible, whose net effect is to change the gravitational potential.

4.2. The basic notation

Let $\rho_L(r)$ be the density distribution of luminous matter, and $\overline{\rho}_L(r)$ its mean value within the sphere of radius r. Originally this material is in form of gas and it is gradually turned into stars so that at each time $\overline{\rho}_L(r,t) = \overline{\rho}_s(r,t) + \overline{\rho}_g(r,t)$, with obvious meaning of the symbols. The masses of luminous material, gas and stars within the sphere of radius r are simply given by

$$M_L(r) = \overline{\rho}_L(r) \times V(r)$$

$$M_g(r,t) = \overline{\rho}_g(r,t) \times V(r)$$

$$M_s(r,t) = \overline{\rho}_s(r,t) \times V(r)$$

where $V(r)$ is the volume of the sphere, supposedly constant in time.
In the following galaxies are identified by their total luminous mass $M_{L,T}$, whereas the luminous mass within the R_e-sphere is named M_{L,R_e}. All masses are in units of $10^{12} \times M_\odot$.
Limited to the R_e-sphere, let us now define the a-dimensional variables

$$G_g(r,t) = \frac{M_g(r,t)}{M_{L,R_e}} = \frac{\overline{\rho}_g(r,t)}{\overline{\rho}_{L,R_e}}$$

$$G_s(r,t) = \frac{M_s(r,t)}{M_{L,R_e}} = \frac{\overline{\rho}_s(r,t)}{\overline{\rho}_{L,R_e}}$$

where $\overline{\rho}_{L,R_e}$ is the mean density of luminous mass within it.
Finally, we introduce the gas components $G_{g,i}(r,t) = G_g(r,t) \times X_i(r,t)$ where $X_i(r,t)$ are the abundances by mass of the elemental species i. Summation of $X_i(r,t)$ over all components is equal to unity.

4.3. The spatial distribution of $M_{L,T}$ and $M_{D,T}$

Luminous matter. The spatial distribution of the luminous matter is supposed to follow the Young (1976) density profile based on the $r^{1/4}$-law. Given the effective radius of a galaxy, one can immediately derive from the tabulations of Young (1976) the density $\rho_L(r)$, the mean density $\overline{\rho}_L(r)$ within the sphere of radius r, and the gravitational potential $\varphi_L(r)$.

Dark matter. The mass distribution and gravitational potential of the dark matter are derived from the density profiles by Bertin et al. (1992) and Saglia et al. (1992) adapted to the Young formalism for the sake of internal consistency. The details of this procedure are given in TCBMP98. In brief we start from the density law

$$\rho_D(r) = \frac{\rho_{D,0} \times r_{D,0}^4}{(r_{D,0}^2 + r^2)^2} \tag{15}$$

where $r_{D,0}$ and $\rho_{D,0}$ are two scale factors of the distribution.

We assume $r_{D,0} = \frac{1}{2} R_{D,e}$, where $R_{D,e}$ is the effective radius of dark matter. Furthermore, for this latter we assume that it scales according to the same law as for the total radii of dark and luminous matter, i.e. $R_{D,e} = \frac{\zeta}{2} R_e = \frac{5}{2} R_e$.

The density scale factor $\rho_{D,0}$ is derived from imposing that the total mass of dark-matter $M_{D,T} = \zeta M_{L,T}$, where $M_{D,T}$ is given by:

$$M_{D,T} = 4\pi \int_0^\infty r^2 \rho(r) dr = 4\pi \rho_{D,0} r_{D,0}^3 m(\infty) \tag{16}$$

with

$$m(\infty) = \int_0^\infty \frac{r^2}{r_{D,0}^3 \left(1 + \left(\frac{r}{r_{D,0}}\right)^2\right)^2} dr \tag{17}$$

for which a numerical integration is required. Finally, the density profile of dark-matter is

$$\rho_D(r) = \frac{M_{D,T}}{m(\infty)} \frac{1}{4\pi r_{D,0}^3} \frac{1}{\left(1 + \left(\frac{r}{r_{D,0}}\right)^2\right)^2}. \tag{18}$$

The radial dependence of the dark-matter gravitational potential is

$$\varphi_D(r) = -G \int_0^r \frac{M_D(r)}{r^2} dr \tag{19}$$

which upon integration becomes

$$\varphi_D(r) = -4\pi G \rho_{D,0} r_{D,0}^2 \widetilde{\varphi_D}\left(\frac{r}{r_{D,0}}\right) \tag{20}$$

where $\widetilde{\varphi_D}\left(\frac{r}{r_{D,0}}\right)$ is given by

$$\int_0^{r/r_{D,0}} \frac{m(r/r_{D,0})}{r_{D,0}\left(\frac{r}{r_{D,0}}\right)^2} dr \tag{21}$$

which must be integrated numerically. Finally, the total binding energy of the gas is

$$\Omega_g(r,t) = \overline{\rho}_g(r,t) V(r) \varphi_L(r) + \overline{\rho}_g(r,t) V(r) \varphi_D(r). \tag{22}$$

4.4. The mass-effective radius relation

To proceed further we need to adopt a suitable relationship between the effective radius and the total mass of the luminous material. For the purposes of this study, we derive from the data of Carollo & Danziger (1994a,b), and Carollo et al. (1993, 1995) the following relation

$$R_e = 17.13 \times M_{L,T}^{0.557} \tag{23}$$

with R_e in kpc and $M_{L,T}$ in units of $10^{12} M_{\odot}$.
Another useful relation is between the total radius and total mass of the luminous material for which using the same sources of data we get

$$R_L = 39.10 \times M_{L,T}^{0.402} \tag{24}$$

in the same units as above.

4.5. The chemical equations

The chemical evolution of elemental species is governed by the same set of equations as in TCBF96 and TCBMP98 however adapted to the density formalism and improved as far as the ejecta and the contribution from the Type Ia and Type II supernovae are concerned (cf. Portinari et al. 1998).

Specifically, we follow in detail the evolution of the abundance of thirteen chemical elements (H, ^{4}He, ^{12}C, ^{13}C, ^{14}N, ^{16}O, ^{20}Ne, ^{24}Mg, ^{28}Si, ^{32}S, ^{40}Ca, ^{56}Fe, and the isotopic neutron-rich elements nr obtained by α-capture on ^{14}N, specifically ^{18}O, ^{22}Ne, ^{25}Mg). Furthermore, the stellar yields in usage here take into account the effects of different initial chemical compositions (cf. Portinari et al. 1998).

The equations governing the time variation of the $G_i(r,t)$ and hence $X_i(r,t)$ are:

$$\frac{dG_i(r,t)}{dt} = -X_i(r,t)\Psi(r,t) +$$

$$\int_{M_{min}}^{M_{B_m}} \Psi(t-\tau_M) Q_{M,i}(t-\tau_M)\phi(M)dM +$$

$$A \int_{M_{B_m}}^{M_{B_M}} \phi(M)[\int_{\mu_{min}}^{0.5} f(\mu)\Psi(t-\tau_{M_2}) Q_{M,i}(t-\tau_{M_2})d\mu] +$$

$$(1-A) \int_{M_{B_m}}^{B_M} \Psi(t-\tau_M) Q_{M,i}(t-\tau_M)\phi(M)dM +$$

$$\int_{M_{B_M}}^{M_{max}} \Psi(t-\tau_M) Q_{M,i}(t-\tau_M)\phi(M)dM \tag{25}$$

where all the symbols have their usual meaning. Specifically, $\Psi(t)$ is the normalized rate of star formation, $Q_{M,i}(t)$ are the restitution fractions of the elements i from stars of mass M (cf. Talbot & Arnett 1973), $\phi(M)$ is the IMF, whose lower and upper mass limits are M_{min} and M_{max} (see below), τ_M is the lifetime of a star of mass M.

The various integrals appearing in Eq. (25) represent the separated contributions of Type II and Type Ia supernovae as introduced by Matteucci & Greggio (1986). In particular, the second integral stands for all binary systems having the right properties to become Type Ia supernovae. M_{Bm} and M_{BM} are the lower and upper mass limit for the total mass of the binary system, $f(\mu)$ is the distribution function of their mass ratios and μ_{min} is the minimum value of this, finally A is the fraction of such systems with respect to the total. We adopt $M_{Bm} = 1.5 M_{\odot}$, $M_{BM} = 12 M_{\odot}$, and $A = 0.2$. The stellar ejecta are from Marigo et al. (1996, 1998), Portinari (1995), and Portinari et al. (1998) to whom we refer for all details. Finally, using the tabulations by Bertelli et al. (1994) we account for the dependence of τ_M on the initial chemical composition.

4.6. The star formation rate

The rate of star formation (SFR) is assumed to depend on the gas density according to the Schmidt (1959) law (see also Larson 1991):

$$\frac{d\overline{\rho}_g(r,t)}{dt} = \nu(r,t)\overline{\rho}_g(r,t)^{\kappa} \tag{26}$$

where the specific efficiency of star formation $\nu(r,t)$ is a suitable function to be specified below. Owing to the uncertainty on the exponent κ (cf. Kennicutt 1998 and references therein), we will calculate models for both $\kappa = 1$ and $\kappa = 2$.
Upon normalization, the star formation rate becomes

$$\Psi(r,t) = \nu(r,t)[\overline{\rho}_{L,R_e}]^{k-1} G_g(r,t)^k. \tag{27}$$

4.7. Mass limits of the IMF

Although the IMF of Padoan et al. (1997) is self-normalizing to unity over the whole range of masses from zero to infinity (cf. Eq. 6), we prefer to limit the mass range of validity from $M_{min} = 0.07 M_{\odot}$ to $M_{max} = 100 M_{\odot}$, values that are likely more suited to real stars, and re-normalize the IMF by imposing that

$$\int_{M_{min}}^{M_{max}} C\phi(M)dM = 1 \tag{28}$$

where

$$C = \frac{1}{1 - \int_0^{M_{min}} \phi(M)dM - \int_{M_{max}}^{\infty} \phi(M)dM} \tag{29}$$

4.8. The energy equation

In order to calculate the IMF we need to derive the density, temperature and velocity dispersion Σ_g of the collapsing clouds. These quantities are obtained by means of a suitable thermal model of the star forming process and the resolution of the energy equation

$$\frac{dE(T,\rho_g,t)}{dt} = H_R(T,\rho_g,t) + H_M + H_C - \frac{\Lambda(T,\rho_g,t)}{\rho_g} \tag{30}$$

where $E(T, \rho_g, t)$ is the energy input per unit mass, H_R, H_M and H_C are the heating rates (per unit mass) of radiative, mechanical, and collapse origin, respectively, and Λ is the cooling rate (in units of $\mathrm{ergs\ cm^{-3}\ s^{-1}}$).

All physical quantities are functions of time and position. Therefore, the IMF continuously varies with time, radial distance, and galaxy mass. The coupling of energy equation with those governing the chemical model and the IMF, in particular, is described in Sect. 5 below.

4.9. Galactic winds

Depending on the competition between heating and cooling, the energy stored into the interstellar medium continuously grows thus making gas hotter and hotter. The case can be met in which the thermal energy of the gas eventually exceeds its gravitational binding energy

$$E_{th}(t) \geq \Omega_g(t) \tag{31}$$

5. Sources of heating and cooling

5.1. Heating

Heating of the interstellar medium is caused by many processes among which we consider the thermalization of the energy deposit by supernova explosions (both Type I and II) and stellar winds from massive stars, the ultraviolet flux from massive stars, and finally two sources of mechanical nature.

Supernovae. The rate of supernova explosions $R_{SNI,II}(t)$ over the time interval Δt is calculated according to standard prescriptions (cf. BCF94, TCBF96, TCBMP98, and Greggio & Renzini 1983 for Type I SN in particular). Knowing the amount of energy released by each SN explosion, the total energy injection over the time interval Δt centered at age t is the sum of the two terms E_{SNI} and E_{SNII} of type

$$E_{SNI,II} = \int_{\Delta t} \epsilon_{SNI,II}(t - t') R_{SNI,II}(t') dt' \tag{32}$$

where $R_{SNI,II}(t)$ is the number of supernovae per unit galactic mass and time, and $\epsilon_{SNI,II}(t)$ is the thermalization law of the energy released by a SN explosion, in which the effects of cooling are suitably taken into account, cf. BCF94, TCBF96, TCBMP98, and Gibson (1995).

Stellar winds. The rate of energy injection by stellar winds is

$$E_W = \int_{\Delta t} \epsilon_W(t - t') R_W(t') dt' \tag{33}$$

where R_W is the number of stars per unit galactic mass and time expelling their envelopes during the time interval Δt and, in analogy with the SN remnants, $\epsilon_W(t)$ is the thermalization law of the kinetic energy of stellar winds. A losing mass star is expected to deposit into the interstellar medium the energy

$$\epsilon_{W0} = \eta_W \times \frac{M_{ej}(M)}{2} (\frac{Z}{Z_\odot})^{0.75} \times v(M)^2 \tag{34}$$

where $M_{ej}(M)$ is the amount of mass ejected by each star of mass M, $v(M)$ is the velocity of the ejected material, and η_W is an efficiency factor of the order of 0.3 (Gibson 1994 and references therein). For the velocity $v(M)$ we take the maximum between the terminal velocity of the wind and the galaxy velocity dispersion Σ. For the cooling law $\epsilon_W(t)$ one could adopt the same formalism as in BCF94.

Ultraviolet flux from massive stars. The rate of energy injection from the ultraviolet flux emitted by massive stars, whose mass is the range $10 \div 100\ M_\odot$, is

$$E_{UV} = \int_{\Delta t} \epsilon_{UV}(t - t') R_{UV}(t') dt' \tag{35}$$

where R_{UV} is the number of massive stars per unit galactic mass and time and ϵ_{UV} is the amount of ultraviolet energy emitted by such stars. To derive a reasonable estimate of the UV flux we adopt the following procedure. The problem is simplified considering that significant fluxes of UV radiation will be emitted only by evolutionary stages at high effective temperature. Therefore we limit ourselves to stars along the main sequence for which the relations between mass, luminosity, and effective temperature are known from stellar model calculations (cf. Bertelli et al. 1994). For each value of the star mass we integrate the spectral energy distribution up to the 2000 Å and calculate its ratio to the total bolometric luminosity, shortly indicated by F_{UV}. The UV flux emitted by each star is therefore

$$\epsilon_{UV} = \eta_{UV} \times F_{UV} \times \langle \frac{L}{L_\odot} \rangle L_\odot \tag{36}$$

where $\langle L/L_\odot \rangle$ is the mean luminosity of a massive star in solar units (the mean is performed over the main sequence phase), and η_{UV} is an efficiency parameter. The fraction F_{UV} increases from about 0.7 to 0.9 as the stellar mass increases from 10 to $100 M_\odot$. The effects of different chemical composition are neglected here. Furthermore, the relationship between mass and lifetime of the star is used to calculated the integral of Eq. (35). The major problem with the UV radiation is whether or not it must be included in the energy balance equation. In presence of dust, nearly all UV radiation is absorbed and re-emitted in the far infrared so that it can freely escape from the galaxy; indeed, the recent models of population synthesis from the far UV to the far infrared by Bressan et al. (1998) and Granato et al. (1997) show that about 99% of the UV radiation is re-processed in presence of even a modest amount of dust. On the basis of the above considerations, only 0.01% of ϵ_{UV} above is injected into the energy equation and, accordingly, $\eta_{UV} = 0.01$. As long as the fraction of UV radiation going directly into the energy equation is as small as 0.01 or so there is not significant effect on the final results.

Perhaps the most important use of the UV radiation is to set a new condition for the occurrence of galactic winds. Knowing the amount of UV flux we calculate the radius of the Stroemgren sphere and associated gas mass, in which 99% of the UV flux is absorbed and re-emitted in the infrared. When the mass of the Stroemgren sphere equals the total gas mass, no further

absorption of the UV radiation is possible, so that the whole UV energy becomes suddenly available to the gas. Many numerical tests proved that, soon after, the thermal energy of the gas gets so high to exceed the gravitational energy so that condition (31) applies.

Remarks on ϵ_{SN} and ϵ_W. According to standard prescriptions for $\epsilon_{SN}(t)$, the thermalization time scale of SN energy is short (a few 10^6 yr) compared to the typical time scale of chemical and photometric evolution (a few 10^7 to 10^8 yr). This means that only supernovae exploding in the recent past will basically contribute to the current energy injection. This allows us to simplify the calculation of the energy input and to treat SN cooling by means of Eq. (30). The same considerations apply to stellar winds, for which the main source of energy are massive stars with short lifetimes and terminal velocities up to 2000 - 3000 km/s. Therefore, we drop the time dependence both in $\epsilon_{SNI,II}$ and ϵ_W. They are set equal to the initial energy of explosion or wind respectively. Sufficiently small time intervals Δt secure the desired accuracy and the recovery of results very close to those obtained with the standard treatment.

Total radiative heating. The total heating rate $H_R(T,\rho,t)$ of Eq. (30) is

$$H_R(T,\rho_g,t) = \frac{E_{SNI} + E_{SNII} + E_W + E_{UV}}{\Delta t}. \quad (37)$$

Mechanical sources. In addition to this, we include two other sources of heating whose origin is of mechanical nature (i.e H_C and H_M to be defined below).

Initial flame. The first term, H_C, is related to the very initial period of galaxy formation, when gas is collapsing with the infall time scale to form the galaxy and star formation has likely not yet started. To evaluate this term in a simple fashion we follow Binney & Tremaine (1987).

Let R_h be the initial radius of the proto-galaxy (say $R_h = 100 \times R_e$) and τ_{ff} the corresponding free-fall time scale

$$\tau_{ff} = \pi\sqrt{\frac{R_h^3}{2GM}} \quad (38)$$

where M is the total mass of the galaxy, i.e. $M_{L,T} + M_{D,T} = (1+\zeta) \times M_{L,T}$. In absence of energy sources of any type, a proto-galactic cloud at the virial temperature would have cooled on a time scale

$$\tau_{cool} = 6.3 \times 10^5 (R_h/10kpc)^2 \qquad \text{yr}. \quad (39)$$

Although the cooling functions at the base of Eq. (39) is somewhat different from the ones is usage here (see below), this is less of a problem because of the marginal role played by this source of energy aimed at providing only the initial flame to start with.

At the end of this very initial phase, the system will retain a fraction of the original energy all the rest being radiated radiated away. A simple estimate of the amount of lost energy is given by the ratio τ_{cool}/τ_{ff}. Therefore, the virial energy and velocity dispersion at the end of this phase are

$$E_{vir} = E_{vir,0}(1 - \frac{\tau_{cool}}{\tau_{ff}}) \quad (40)$$

$$\Sigma = (1 - \frac{\tau_{cool}}{\tau_{ff}})^{0.5}\Sigma_0 \quad (41)$$

where $E_{vir,0}$ and Σ_0 are the initial virial energy and velocity dispersion, respectively. The energy left over at the end of this phase is then converted into heat at the rate (per unit galactic mass and time)

$$H_C = \frac{E_{vir}}{\tau_{ff}} \quad (42)$$

The ratio τ_{cool}/τ_{ff} is derived in the following way: expressing $R_h = \lambda R_e$ and using the relation between the effective radius and the total luminous mass, Eq. (23) above, we get

$$\frac{\tau_{cool}}{\tau_{ff}} = 0.0083 \times (1+\zeta)^{0.5} \times \lambda^{0.5} \times M_{L,T}^{0.78} \quad (43)$$

where $M_{L,T}$ is in units of $10^{12} M_\odot$. For typical $\lambda \simeq 100$, and $\zeta = 5$ we get $\tau_{cool}/\tau_{ff} = 0.48$ and $\tau_{cool}/\tau_{ff} = 0.001$ for the 3 and 0.001 $M_{L,T}$ galaxies, respectively.

This source of energy is supposed to be active as long as the galaxy age is smaller than τ_{ff}, thus providing the initial energy input and gas temperature. The effect of this energy source on the final result is however of marginal importance, which somehow justifies the crudeness of the present approach.

Cloud-cloud collisions. The second term H_M owes its origin to mechanical interactions of different nature among gas clouds, such as shock waves, friction, cosmic rays, etc. In order to get an estimate of this source of energy from simple arguments, we have looked at the cloud-cloud collisions. Limiting to the case of head-on collisions, the kinetic energy per unit mass of the relative motion is Σ^2 (galaxy velocity dispersion), whereas the number of such collisions per unit time can be simply expressed by $1/t_{ff}$, where t_{ff} is the current free-fall time scale. Therefore the rate of energy injection is cast as follows

$$H_M = \eta_M \times \frac{\Sigma^2}{t_{ff}} \quad (44)$$

where η_M is an efficiency parameter masking the real complexity of the energy injection by mechanical interactions. Preliminary test calculations show that the parameter η_M ought to be of the order of 10^{-6}. This source of energy actually plays the dominant role in the models we are going to describe because it will turn out to drive the minimum temperature attainable by the collapsing gas clouds (see below).

The CBR limit. Although not explicitly included in Eq. (30), there is another source of heating to be considered, i.e. the cosmic background radiation (CBR). It is used to limit the lowest temperature attainable by gas as a consequence of cooling. Specifically, we assume that at each time the gas temperature cannot be cooler than the limit T_{CBR} set by

$$T_{CBR}[z(t)] = \frac{273}{100} \times [1 + z(t)] \quad (45)$$

where $z(t)$ is the red-shift corresponding to the galactic age t. The red-shift $z(t)$ depends on the choice of the cosmological

model of the Universe, i.e. H_0, q_0 (Hubble constant and deceleration parameter, respectively, in a Friedmann model), and red-shift of galaxy formation z_{for}. All of the results below are for the case of $H_0 = 50\,\mathrm{km\,s^{-1}\,Mpc^{-1}}$, $q_0 = 0$, and $z_{for} = 5$.

5.2. Cooling

The cooling term $\Lambda(T, \rho_g, t)$ of Eq. (30) is derived from literature data, and it includes several radiative processes. For temperatures greater than 10^4 K we lean on the Sutherland & Dopita (1993) tabulations for a plasma under equilibrium conditions and metal abundances [Fe/H]=-10 (no metals), -3, -2, -1.5, -1, -0.5, 0 (solar), and 0.5. For temperatures in the range $100 \le T \le 10^4$ the dominant source of cooling is the H_2 molecule getting rotationally or vibrationally excited through a collision with an H atom or another H_2 molecule and decaying through radiative emission. The data in use have been derived from the analytical expressions of Hollenbach & McKee (1979) and Tegmark et al. (1996). Finally, for temperatures lower than 100 K, starting from the relation of Theis et al. (1992) and Caimmi & Secco (1986), we have implemented the results of Hollenbach & McKee (1979), and Hollenbach (1988) for CO as the dominant coolant. The following analytical relation in which the mean fractionary abundance of CO is given as a function of [Fe/H], is found to fairly represent the normalized cooling rate (i.e. Λ_{CO}/n^2 with n the number density of particles)

$$\frac{\Lambda_{CO}}{n^2} = 1.6 \times 10^{-29} 10^{([Fe/H]-1.699)} T^{0.5} \quad \mathrm{erg\,cm^{-3}\,s^{-1}} \quad (46)$$

The net cooling rate ($\Lambda \times n^2$) over the whole temperature range is shown in Fig. 2, in which the effects of metallicity are clearly visible. The number density in usage for the purposes of Fig. 2 is $n \simeq 10$. It is worth mentioning that no re-scaling of the cooling rate from the various sources has been applied to get the smooth curves shown in Fig. 2.

How does Eq. (30) compare with respect to the classical cooling laws for supernova ejecta ? To answer this question we display in Fig. 3 the path in the energy-cooling time plane followed by supernova ejecta according to the most recent discussion of the subject by Gibson (1995) and one of the models we are going to present below, i.e. the 3 $M_{L,T}$ galaxy during its stages of stellar activity. The cooling laws of supernova ejecta displayed in Fig. 3 are for different metallicities as indicated, typical density of the medium of about 10^{-22} g/cm^3, and injected energy of 10^{51} erg. In the model galaxy the metallicity is about $Z = 0.010$, the parameter of H_M is $\eta_M = 2 \times 10^{-6}$, the density is about 10^{-23} g/cm^3, and the energy injected is about 10^{11} erg per unit mass of gas. Re-normalization of the energies is applied. Remarkably, the general trend is similar to that of supernova cooling laws, at least as far as the drop-off is concerned, and the cooling time is comprised between those of the $Z = 0.001$ and $Z = 0.020$ cases.

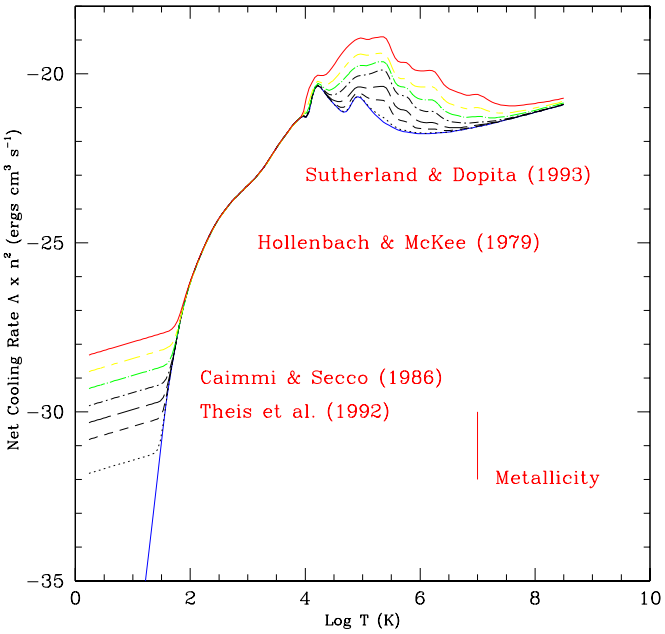

Fig. 2. The net cooling rate $\Lambda \times n_j n_k$ in $\mathrm{ergs\,cm^3\,s^{-1}}$ as a function of temperature: from Sutherland & Dopita (1993) for $T \ge 10^4$, Hollenbach & McKee (1979) and Tegmark et al. (1996) for $100 \le T \le 10^4$, and Caimmi & Secco (1986) and Theis et al. (1992) for $T < 10^2$ K. The product $n_j \times n_k$ contains the number densities of particles. The meaning of n_j and n_k changes according to the portion of the curve under consideration: in Sutherland & Dopita (1993) $n_j \times n_k = n_e \times n_i$, where n_e and n_i are the number densities of electrons and sum of the ion number densities, respectively. In all the others, the product $n_j \times n_k = n^2$, with n the number density of all particles lumped together for the sake of simplicity. The number density in usage is $n \simeq 10$. From bottom to top, each curve corresponds to an increasing value of the metallicity [Fe/H]. See the text for more details.

6. The thermal model

In order to derive temperature, density and velocity dispersion of the star forming clouds undergoing fragmentation according to the adopted IMF, one has to adopt a thermal model for the star forming process. This is sketched as follows:

- During each time step Δt, the energy input from the various sources heats up and expands the gas, whereas cooling acts in the opposite sense.
- Eq. (30) is integrated in time assuming that heating-expansion and cooling-contraction of gas follow the constant-pressure law

$$P = \frac{K}{\mu H} \rho T = const \quad (47)$$

  with obvious meaning of the symbols.
- An equilibrium stage with temperature T_{eq} and density $\rho_{g,eq}$ is soon reached that yields the Jeans mass $M_{J,eq}$ above which elemental gas clouds are gravitationally unstable and prone to collapse.
- In principle we can suppose that of the existing clouds only the fraction whose Jeans mass is larger than $M_{J,eq}$ can form

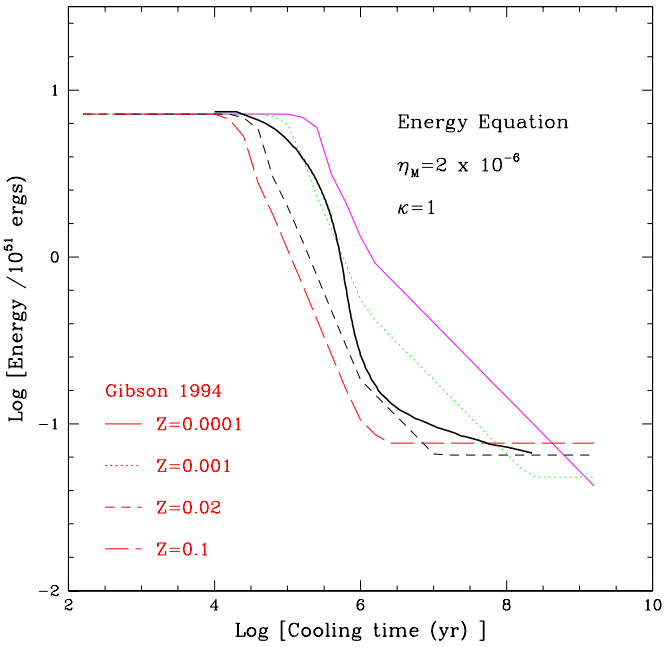

Fig. 3. Cooling law of supernova remnants $\epsilon_{SN}(t)$ from Gibson (1994). Each curve is for a different metallicity of the interstellar medium as indicated. Superposed is the cooling law of Eq. (30) for the 3 $M_{L,T}$ model with age of 0.024 Gyr and mean metallicity $\langle Z \rangle = 0.010$ (thick line) described in the text. Re-normalization of the input energies is applied.

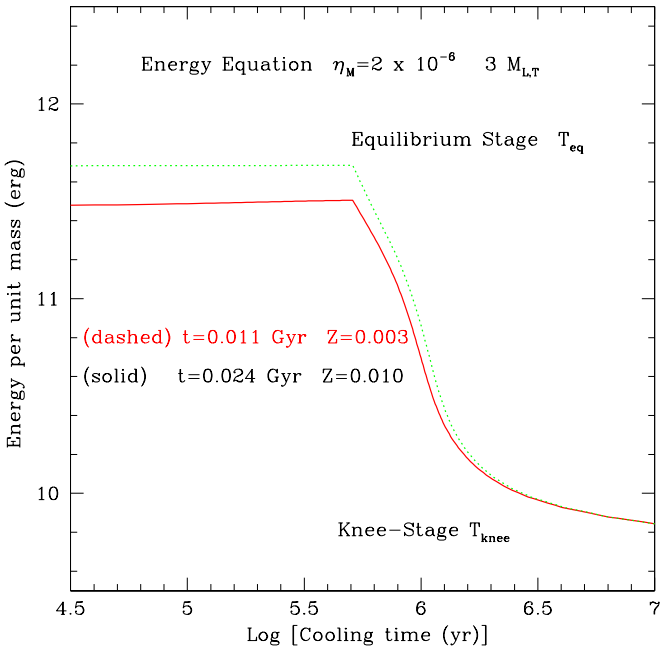

Fig. 4. The cooling law the 3 $M_{L,T}$ model with $\nu = 10$. Each curve corresponds to a different age and metallicity. The galactic age (in Gyr) is indicated. The particular stages at which the equilibrium temperature (T_{eq}) is reached and rapid contraction (collapse) begins, and the final temperature (T_{knee}) at which fragmentation is supposed to occur are indicated. See the text for more details.

stars. In order to determine the temperature, density and velocity dispersion at the start of the star forming process we need to follow the thermo-dynamical fate of the gas component prone to instability. This is conceived as thermally decoupled from the surrounding medium, so that no further energy input of radiative nature is possible, but still able to mechanically interact with it. Therefore, the radiative term $H_R(T, \rho_g, t)$ of Eq. (30) is switched off, whereas the mechanical term H_M is retained.

– The fraction of gas with Jeans mass in excess of $M_{J,eq}$ is let cool down and collapse until a new equilibrium stage is reached characterized by certain values of temperature and density, T_{knee} and ρ_{knee}, respectively. The existence of the *knee-stage* is secured by the energy input of mechanical nature. In any case, T_{knee} is not let be lower than $T_{CBR}[z(t)]$. In such a case the integration of the energy equation is stopped, and T_{knee} and ρ_{knee} are the last computed values.
– During all these stages the cooling and free-fall times scales turn out to be nearly identical. The temporal evolution of the gas energy (per unit mass of gas) is shown in Fig. 4 for two different evolutionary models of the the $3M_{L,T}$ galaxy. Along the curves we indicate the equilibrium and *knee* stages at which the temperatures T_{eq} and T_{knee} are defined. The efficiency of star formation characterizing this model will be defined below.
– We identify the fraction of gas that undergoes the cooling process described above and is able to reach T_{knee} and ρ_{knee} as the molecular component in which fragmentation can occur according to the Padoan et al. (1997) scheme.
– It is reasonable to assume that these clouds acquire their kinetic energy from the energy budget of the surrounding medium. Denoting with $E_{th,knee}$ the thermal energy of the collapsing gas at the knee-stage, the corresponding velocity dispersion of this can be expressed as

$$\Sigma_g(T_{knee}) = \sqrt{\frac{2 \times E_{th,knee}}{M_J(T_{knee})}} \tag{48}$$

– Finally, the temperature and density T_{knee} and ρ_{knee}, and the velocity dispersion $\Sigma_g(T_{knee})$ are the values to be plugged into the IMF. Each cloud prone to star formation will fragment into stars according to this IMF.
– The case may arise, in which for the values of T_{knee}, ρ_{knee}, and velocity dispersion $\Sigma_g(T_{knee})$ derived from the energy equation the peak mass of the IMF is comparable or even lower than the minimum mass $M_{min} = 0.07 M_\odot$ for the existence of real stars (i.e. burning hydrogen in their cores). In such a case the peak mass is not let fall below $M_l = 0.1 M_\odot$, and the IMF is calculated with the temperature obtained from inverting Eq. (10) in which ρ_{knee} and $\Sigma(T_{knee})$ are used. Even if there is a marginal inconsistency, this can be neglected for any practical purpose.

Table 1. Basic data of the models. $M_{L,T}$ and M_{L,R_e} are the total luminous mass and the mass within the effective radius, respectively. They are in units of $10^{12} \times M_\odot$. $\langle\rho\rangle$ is the mean mass density (in $gr\ cm^{-3}$) within the R_e-sphere. Σ is the galaxy velocity dispersion. T_{knee} and M_P are the maximum values of T_{knee} (in K) and peak mass (in $M_\odot$) of the IMF in the course of galactic evolution. t_w is the age (in Gyr) of the galaxy at the onset of galactic wind. $M_g/M_{L,R_e}$ and $Ms/M_{L,R_e}$ are the fractionary masses of gas and stars, respectively, at the galactic wind stage. Z and $\langle Z\rangle$ are the current and mean metallicity reached by the galaxy at the wind stage.

$M_{L,T}$	M_{L,R_e}	ρ	Σ	T_{knee}	M_P	t_w	$\frac{M_g}{M_{L,R_e}}$	$\frac{M_s}{M_{L,R_e}}$	Z	$< Z >$	Mg_2
			Set A	$\kappa = 1$	$\eta_M = 2 \times 10^{-6}$						
3	1.2420	1.33(-23)	354	43.3	1.030	0.24	0.256	0.657	0.0815	0.0452	0.3364
1	0.4140	2.79(-23)	278	42.6	0.809	0.40	0.120	0.766	0.1031	0.0505	0.3430
0.1	0.0410	1.31(-22)	167	38.0	0.553	0.53	0.052	0.855	0.0765	0.0298	0.3120
0.01	0.0041	6.16(-22)	100	33.9	0.420	0.72	0.021	0.906	0.0552	0.0155	0.2736
0.001	0.0004	2.89(-21)	60	29.7	0.307	0.83	0.011	0.941	0.0421	0.0060	0.2182
			Set B	$\kappa = 1$	$\eta_M = 3 \times 10^{-6}$						
3	1.2420	1.33(-23)	354	47.8	1.420	0.21	0.308	0.606	0.0798	0.0492	0.3414
1	0.4140	2.79(-23)	278	43.9	0.884	0.40	0.121	0.760	0.1076	0.0554	0.3484
0.1	0.0410	1.31(-22)	167	38.0	0.560	0.50	0.058	0.849	0.0757	0.0311	0.3145
0.01	0.0041	6.16(-22)	100	33.9	0.424	0.69	0.022	0.905	0.0542	0.0157	0.2746
0.001	0.0004	2.89(-21)	60	30.2	0.329	0.85	0.011	0.939	0.0429	0.0064	0.2216
			Set C	$\kappa = 2$	$\eta_M = 2 \times 10^{-6}$						
3	1.2420	1.33(-23)	354	43.1	1.010	0.85	0.218	0.638	0.1093	0.0567	0.3498
1	0.4140	2.79(-23)	278	42.6	0.799	0.74	0.225	0.648	0.0919	0.0471	0.3488
0.1	0.0410	1.31(-22)	167	38.0	0.549	0.85	0.182	0.718	0.0599	0.0250	0.3018
0.01	0.0041	6.16(-22)	100	33.9	0.417	1.26	0.130	0.780	0.0420	0.0137	0.2665
0.001	0.0004	2.89(-21)	60	29.5	0.300	2.55	0.076	0.827	0.0335	0.0073	0.2293
			Set D	$\kappa = 2$	$\eta_M = 3 \times 10^{-6}$						
3	1.2420	1.33(-23)	354	47.6	1.400	0.73	0.240	0.619	0.1088	0.0617	0.3547
1	0.4140	2.79(-23)	278	44.0	0.869	0.68	0.239	0.636	0.0920	0.0502	0.3426
0.1	0.0410	1.31(-22)	167	38.0	0.554	0.82	0.187	0.712	0.0602	0.0266	0.3054
0.01	0.0041	6.16(-22)	100	33.9	0.422	1.20	0.133	0.779	0.0416	0.0139	0.2673
0.001	0.0004	2.89(-21)	60	30.2	0.327	2.54	0.076	0.825	0.0340	0.0076	0.2319

6.1. Deriving the specific efficiency of star formation

The discussion above has been referred to the fraction of gas with Jeans mass in excess of $M_{J,eq}$ and ready to collapse and fragment into stars. This fraction is, however, still unknown. Indeed to be determined a law governing the mass or number distribution of such clouds is needed. Similarity arguments would suggest that the same IMF governing star formation should also regulate the cloud mass (number) distribution. The major difference is in the temperature, density, and velocity dispersion to be adopted. It goes without saying that T_{eq} and ρ_{eq} must be used as they represent the stage at which elemental clouds become thermo-dynamically distinct units out of the surrounding medium. In such a case, the mass fraction of unstable clouds would be

$$f_{Jeans} = \int_{M_{J,eq}}^{\infty} C\phi(M, T_{eq}, \rho_{g,eq}, \Sigma_g(T_{eq}))dM \qquad (49)$$

In principle, with aid of this quantity one could derive $\nu(r,t)$. Recalling that cooling occurs on a certain time scale τ_{cool}, known from solving Eq. (30), we expect that the rate of star formation will be inversely proportional to τ_{cool}. On the base of the above arguments, we could write the specific efficiency $\nu(r,t)$ of the star formation rate as

$$\nu(r,t) = \nu_0 \times \frac{f_{Jeans}}{\tau_{cool}} \qquad (50)$$

where ν_0 is a suitable scale factor of the order of unity.

With this formulation for $\nu(r,t)$, there would no longer be free parameters in the rate of star formation, which would be tightly coupled to the energy storage of the medium in which stars are born. Star formation drives the energy input, and this latter in turn affects star formation: a self-regulating mechanism is soon established.

The application of the above scheme rises, however, some difficulties both of conceptual and numerical nature. First it is not granted that the number (mass) distribution of unstable clouds is governed by the same law determining the mass distribution of stars at each formation event, second both f_{Jeans}

and τ_{cool} fluctuate from time step to time step, thus rendering the associated value of $\nu(r,t)$ highly uncertain. The preliminary analysis of the problem has shown that the quantity f_{Jeans}/τ_{coll} is of the order of $5 \div 50$. Therefore, we considered the specific efficiency $\nu(r,t)$ as an adjustable parameter to be eventually fixed by comparing model results with observational data (e.g CMR, chemical abundances, etc..) and did not make use of the above scheme.

7. The reference models

In this section we present our reference models for elliptical galaxies of different total luminous mass $M_{L,T}$ and luminous mass $M_{L,Re}$ within the effective radius.

Four sets of models are calculated to explore the effects of different choices of η (the parameter governing the efficiency of the mechanical sources of energy) and κ (the exponent of the star formation law) at fixed ν (the parameter driving the efficiency of the star formation rate). The following values are considered: $\eta_M = 2 \times 10^{-6}$ and $\eta_M = 3 \times 10^{-6}$, $\kappa = 1$ and $\kappa = 2$, and $\nu = 10$.

The four sets of models are presented in Table 1, which lists the total luminous mass $M_{L,T}$, the total luminous mass M_{L,R_e} inside the effective radius, the mean mass density within R_e, the galaxy velocity dispersion Σ, the maximum values of T_{knee} (in K) and peak mass M_P (in $M_\odot$) of the IMF reached in the course of galactic evolution (before the onset of galactic winds), the age t_w (in Gyr) at the onset of the galactic wind, the fractionary masses in gas, $M_g/M_{L,R_e}$, and stars $M_s/M_{T,R_e}$ inside the R_e-sphere at the onset of the wind, the current (Z) and mean metallicity ($\langle Z \rangle$), and finally the index Mg_2 at the same epoch. Most of the discussion below will refer to models of set A with $\kappa = 1$ and $\eta_M = 2 \times 10^{-6}$. Similar considerations will hold also for all remaining models. However, when examining the CMR and FP (Sect. 9 below), we will also take into account the models of the other sets.

7.1. General properties

All the models obey some general properties that are determined by the interplay between the physical conditions of the star forming gas and the IMF. We will sketch the problem in several steps for the sake of an easier understanding:

- Given the initial physical conditions, gas density, velocity dispersion and gas temperature (the one determined by the very first energy source H_C), which depend on the galaxy mass, the initial shape of the IMF is determined. Energy from supernova explosions and stellar winds is soon injected into the interstellar medium making it hotter and hotter. The IMF immediately responds to these variations of the physical conditions. T_{knee} and M_P increase thus making the IMF more skewed towards the high mass end. The process will continue till a sort of equilibrium stage is reached, during which both T_{knee} and M_P remain nearly constant.
- However, at proceeding star formation, the gas gets richer in metals thus increasing the cooling efficiency. A situation is eventually met in which cooling is so efficient that the gas temperature and peak mass of the IMF in turn start decreasing. This implies that less energy is injected into the interstellar medium with consequent catastrophic fall-off of both temperature and peak mass.

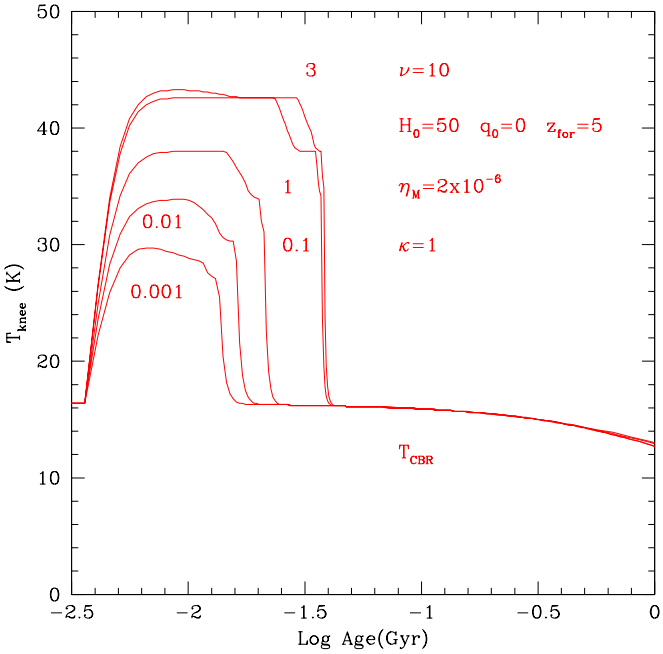

Fig. 5. The gas temperature (in K) as a function of the age (in Gyr) for the models galaxies of set A with $M_{L,T}$ equal to 0.001, 0.01, 0.1, 1 and 3 as indicated. Similar relations are found for all remaining models.

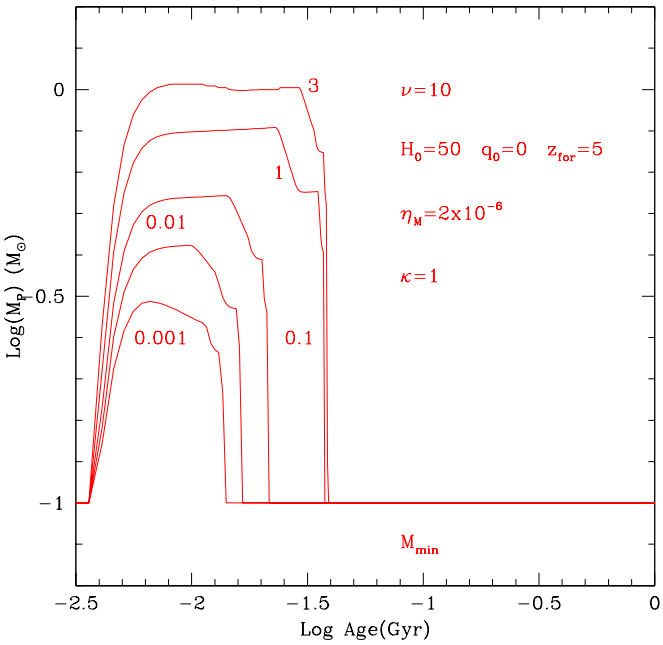

Fig. 6. The peak mass M_P (in solar units) of the IMF as a function of the age (in Gyr) for the models galaxies of set A with $M_{L,T}$ equal to 0.001, 0.01, 0.1, 1 and 3 as indicated. Similar relations are found for all remaining models.

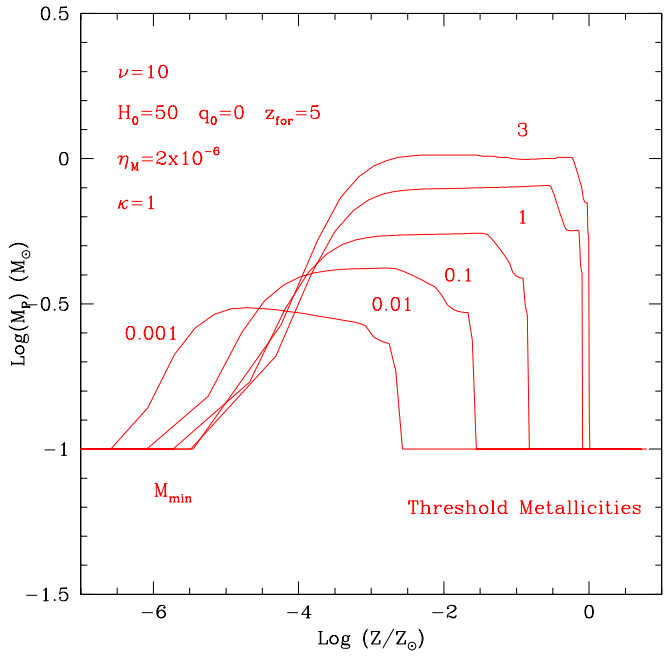

Fig. 7. The variation of the peak mass M_P as a function of the gas metallicity for all models under consideration.

– The above scheme holds for all galaxies, but owing to the different initial conditions (at increasing galaxy mass the mean gas density gets lower, the velocity dispersion gets higher together with the initial gas temperature) in the course of evolution the mean IMF is more skewed toward the high mass end (M_P shifts to higher masses and the slope above it gets slightly flatter) at increasing galaxy mass.

The temporal evolution of the gas temperature, and peak mass is shown in Fig. 5 and Fig. 6, respectively, whereas the relationship between M_P and metallicity is presented in Fig. 7. Notable features of the three diagrams are: (i) the dependence of the maximum value attainable by T_{knee} and M_P on the galaxy mass (both increase with this); (ii) the existence of a threshold value of the metallicity, above which cooling gets so efficient that both T_{knee} and M_P dramatically drop to their minimum permitted values, i.e. $T_{CBR}[z(t)]$ and $0.1 M_\odot$, respectively; (iii) the dependence of the threshold metallicity on the galaxy mass (it gets higher at increasing mass).

7.2. The onset of galactic winds

In all models with $\kappa = 1$, the galactic wind occurs at early epochs, i.e. within the first Gyr, even though a systematic trend with the galaxy mass can be noticed. High mass galaxies undergo their wind ejection earlier than low mass galaxies ($0.21 \div 0.24$ Gyr for the $3M_{L,T}$ galaxy and $0.83 \div 0.85$ Gyr for the $0.001 M_{L,T}$ object).

In contrast, models with $\kappa = 2$ first delay the onset of the galactic wind and second span a much wider range of ages. These go from $0.73 \div 0.85$ Gyr for the $3M_{L,T}$ galaxy to 2.55 Gyr for the $0.001 M_{L,T}$ object.

The star formation history of our model galaxies is shown in Fig. 8, whereby the solid and dotted lines are for models of sets A and C, respectively. The rate of star formation, in units of $M_{L,Re} \times 10^{12} \times M_\odot / pc^3 / Gyr$, is plotted against the age (in Gyr). For the sake of clarity, we limit the age to the first 10 Gyr. With the efficiency of star formation we have assumed ($\nu = 10$) most of the gas is turned into stars within the first few 10^8 years with consequent fall-off of the gas content and star formation rate.

The time variation of the gas content is shown in Fig. 9 where one can notice that even in models with somewhat prolonged activity, the amount of gas left over after the first 0.5 Gyr is rather small. After the minimum in each curve, which corresponds to the galactic wind stage, the gas content rises again because continuously ejected (into the interstellar medium) by dying stars. However, as star formation does no longer occur in our models, this gas is supposed to freely escape into the intergalactic medium, because it is rapidly heated up to high temperatures corresponding to the velocity dispersion of the galaxy (cf. Fabbiano 1986).

What is the reason for the different behavior between models A and C or B and D ? and how much do the models of the four groups differ each other ? Close inspection of their structure shows that there is no significant difference among them, the only reason for the difference in t_w being the different temporal behaviour of the star formation rate as a function of κ.

It is worth emphasizing that in both cases the relationship between galaxy mass and age of the galactic wind has the opposite trend as compared to the standard supernova driven galactic wind model (cf. Sect. 1) in which low mass galaxies eject their wind much earlier than the high mass ones. We will come back later to this point.

7.3. Which wedge to the energy equation? The role of η_M

As already anticipated, the term H_M of the energy equation (together with the CBR limit) has an important role on determining the properties of the models. Why and how are easy to understand. They indeed provide a lower limit to the temperature attainable by the gas during the cooling process. While the effect of $T_{CBR}[z(t)]$ is straightforward, the one of H_M is by far more indirect and difficult to understand. This term is constant for a given galaxy because so are Σ and t_{ff}, but it varies from galaxy to galaxy. According to its definition, it represents a threshold value for the energy input below which gas clouds prone to collapse cannot go. Were this term neglected, owing to the efficiency of cooling (in presence of metals, in particular), gas clouds would fall down to extremely low temperatures on a very short time scale. Since the peak mass of the IMF scales with temperature, H_M has a direct effect on M_P and mean slope of the IMF above it. The higher H_M, the higher is M_P and the flatter is the IMF in the mass range above the peak. The quantitative effects depend of course on η_M. If H_M is efficient, and M_P in turn is shifted toward the high mass end (say above $1 M_\odot$), of the generations of stars born under these conditions, a large fraction of these will soon evolve, become white dwarf

or collapsed remnants in virtue of their short lifetime as compared to the evolutionary time scale of a galaxy. More gas is refuelled to the interstellar medium, more metals are created, and star formation will tend to last longer. The extreme case can be met in which, depending on the competition between gas restitution and heating, no galactic wind occurs in all model galaxies. Therefore H_M eventually drives the mean metal content, the relative fraction of living stars and remnants (white dwarfs, neutron stars, black holes as appropriate), and many other properties of the models, e.g. the colors (see below). All this hints that the parameter η_M can perhaps be constrained by looking at global properties either of a galaxy, such as the mean and maximum metallicity, the colors at the present epoch etc., or of a galaxy manifold, such as the CMR. Many preliminary models calculated to this aim have indicated that $\eta_M = 2 \div 3 \times 10^{-6}$ is a plausible choice leading to acceptable models. Other values cannot be excluded.

8. Discussion of the main results

8.1. Star formation history

As a result of the complex game between IMF and gas thermodynamics, the standard supernova driven wind model is largely modified. Recalling that this latter was suggested to explain the CMR as a mass-metallicity sequence (the mean metallicity grows with the galactic mass), from the entries of Table 1 we see that the same trend is now possible even for models in which the overall duration of the star forming decreases when the galaxy mass increases *i.e.* $\Delta t_{SF} \propto M_G^{-1}$ *as indicated by the chemical abundances*. The range spanned by Δt_{SF} cannot be firmly established because of the many uncertainties affecting the models. However, the possibility exists that, following the dominant initial activity of rather short duration, traces of star formation might occur over much longer periods of time. Remarkably, this is easier to get in low mass galaxies than in high mass ones. In this context, an elegant way out can be found to the difficulties encountered by standard models as far as the distribution of nearby galaxies in the H_β versus $[\mathrm{MgFe}]$ plane, the trend in the suspected enhancement of α-elements, and the gradients in H_β and $[\mathrm{MgFe}]$ across a galaxy are concerned (see Sect. 2 and the discussion below). We will see that the standard interpretation of the CMR is maintained as also these models yield the right mass-metallicity sequence. Finally, there is another consequence of the density dependence of the IMF: since within a galaxy the central regions are naturally denser than the external ones, we expect over there the same trend as passing from a low mass (high density) to a high mass (low density) galaxy. Therefore, the central regions of a galaxy should form stars for periods of time longer than their outskirts. If so, galaxies should be built up by an out-in process.

8.2. Luminous versus dark material

Since in the course of evolution, the peak mass of the IMF first grows to a maximum and then declines, and the maximum value can be as high as $1 \div 1.4 M_\odot$, we expect different proportions of living stars and collapsed remnants as a function of time (the present age in particular). In brief, of the many stellar generations formed during the activity period Δt_{SFR}, those with lifetime shorter than $T_G - \Delta t_{SFR}$, where T_G is the current

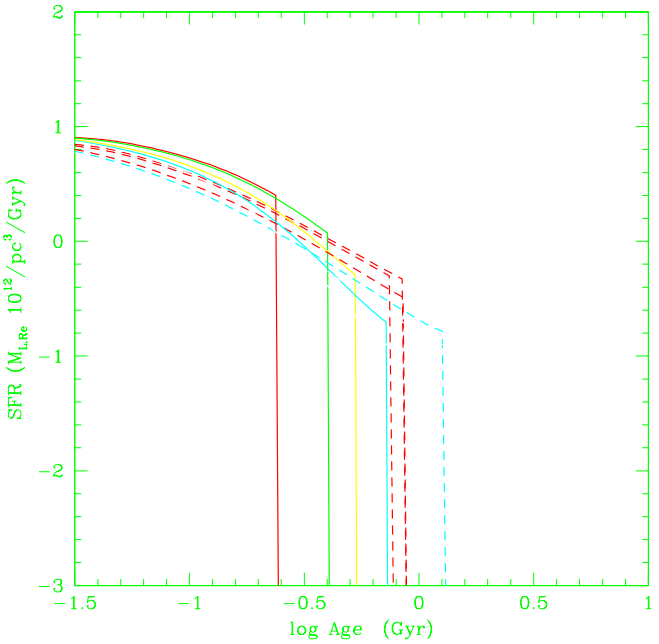

Fig. 8. The normalized rate of star formation SFR as a function of the age for set A (thick solid lines) and C (thin dashed lines) models. The SFR is expressed in units of $M_{L,Re} \times 10^{12} \times M_\odot/pc^3/Gyr$. For the sake of clarity the age is limited to the first 10 Gyr.

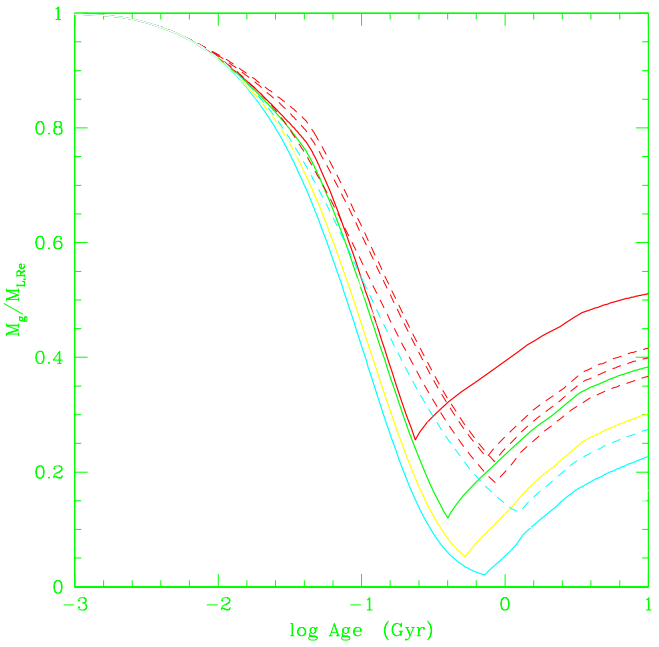

Fig. 9. The fractionary mass of gas as a function of the age for set A (thick solid lines) and set C (thin dashed lines) models. For the sake of clarity the age is limited to the first 10 Gyr.

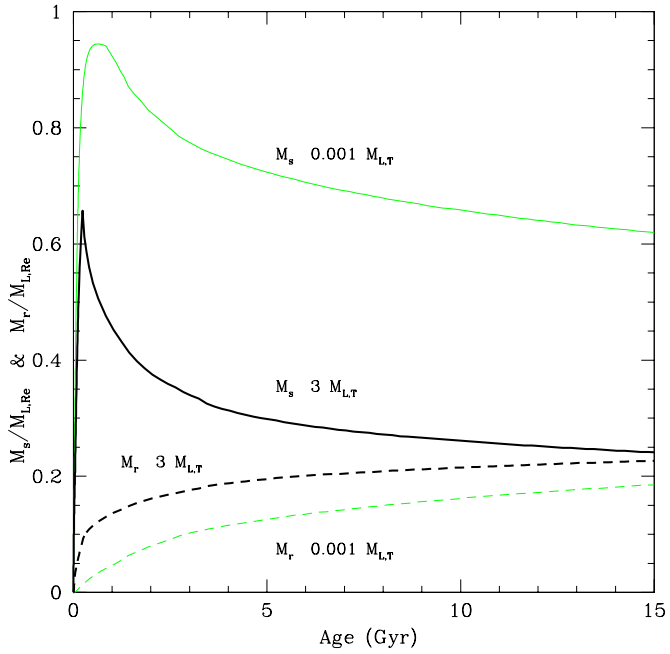

Fig. 10. Fractionary masses in stars (solid lines), and remnants (dashed lines) as a function of the age for the 0.001 $M_{L,T}$ (thin lines) and the 3 $M_{L,T}$ (thick lines) galaxies of set A.

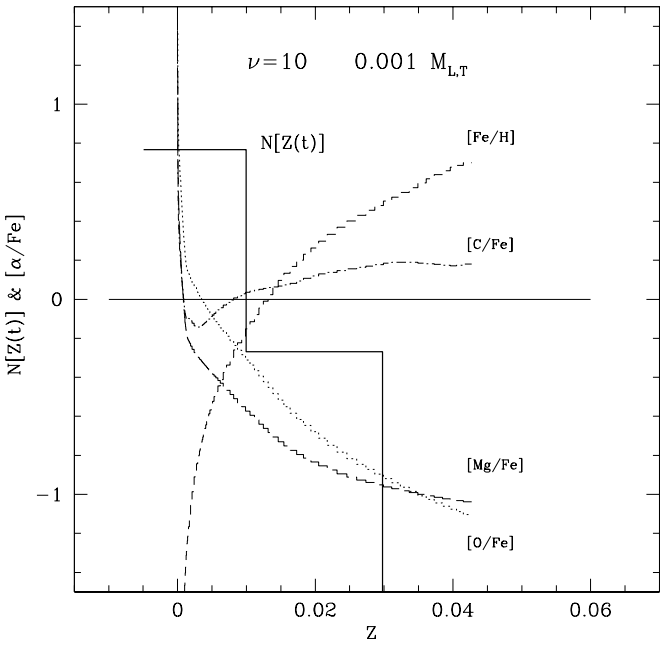

Fig. 11. The relative number distribution of living stars $N[Z(t)]$ per metallicity bin (solid line). $N[Z(t)]$ is on logarithmic scale and in arbitrary units. The relationship between [Fe/H], [C/Fe], [O/Fe], [Mg/Fe], and the total metallicity Z. The galaxy on display is the 0.001 $M_{L,T}$ model of set A at the age of 15 Gyr. The largest fraction of stars in this galaxy have abundance ratios well below solar, this in spite of the short duration of the star forming period (0.82 Gyr). This model is the prototype of a galaxy without enhancement of the α-elements.

galactic age, are now in collapsed remnants (black holes, neutron stars, white dwarfs as appropriate to the initial star mass). They constitute the "baryonic dark matter" scarcely contributing, if nothing at all, to the total light. It goes without saying that the remaining stellar content is in form of visible stars almost fully contributing to the total light. How much mass is present in "baryonic dark matter" ? How does the fractionary value of this mass vary with the galaxy mass (local density and temperature in turn) ? To this aim, in Fig. 10 we plot the fractions of visible stars (solid line) and collapsed remnants (dashed lines) as a function of the age. The corresponding gas fraction was already shown in Fig. 9. For the sake of clarity, we limit ourselves to display only the 0.001 and 3 $M_{L,T}$ galaxies of set A.

It is worth noticing that while the fractionary masses of living stars and gas are calculated with high precision from the set of equations governing chemical evolution, the fractionary mass of remnants is calculated separately with a precision of about 5%. This explains why the sum of the three fractions may sometimes be slightly greater than one ($1 \div 1.05$ in general).

Interestingly enough, in the R_e-sphere of a low mass galaxy (0.001 $M_{L,T}$) about 80% of the original mass $M_{L,Re}$ is in form of visible stars, the rest is in remnants, and there are almost no traces of gas. Conversely, in the same region of a massive galaxy (3 $M_{L,T}$) only 25% of the original mass M_{L,R_e} is now in form of living stars, about 20% of it in form of collapsed remnants, and 55% of it has remained in form of gas partly expelled at the stage of galactic winds and partly continuously ejected by dying stars and never re-used of form stars. For the same arguments advocated to predict the gradient in the duration of the star forming activity across a galaxy, we expect that the fraction of living stars ought to decrease with galactocentric distance. It goes without saying that as a consequence of this, one expects the mass-luminosity ratio to increase with the galaxy mass and the radial distance.

The time dependence of the gas content deserves some final remarks. At the onset of galactic winds, the gas content has reached its minimum value because of the past star formation activity. However, generous amounts of gas are later lost by dying stars. The fractionary mass of the newly emitted gas is significantly larger than what customarily possible with standard, Salpeter-like IMF. Since this gas is likely soon heated up above the virial temperature and lost by the galaxy, it will significantly contribute to enrich and fuel the intra-cluster medium (see below).

8.3. Metallicity and enhancement of α-elements

How do the metallicity and enhancement of α-elements vary as a function of time and galactic mass under this continuously changing IMF ? The answer is provided by Figs. 11 and 12, in which we plot the relative distribution of stars, $N[Z(t)]$, per metallicity bin together with the relationships between [Fe/H], [C/Fe], [O/Fe], and [Mg/Fe], and the total metallicity Z. Fig. 11 refers to the 0.001 $M_{L,T}$ galaxy, whereas Fig. 12 refers to the 3 $M_{L,T}$ object. Both galaxies belong to set A and are displayed at

Table 2. Amounts of mass in form of oxygen and iron ejected into the intra-cluster medium by galaxies of different mass $M_{L,T}$ over their whole life. The data refer to the models of set A with $\kappa = 1$ and $\eta_M = 2 \times 10^{-6}$. The symbol gw indicates the amount of material ejected at the stage of galactic wind. The symbol sw indicates the total amount of material emitted by dying stars from the wind epoch to the present time. Fe_T and O_T are the totals. M_g^{ej} is the total amount of gas thrown into the intra-cluster medium. All masses are in $M_\odot$. y_{Fe} and y_O are crude estimates of the galactic yields of the two elements, i.e. $M_j/M_{L,R_e}$. Finally, O_T/Fe_T is a crude estimate of the degree of α-enhancement in the ejected material.

$M_{L,T}$	M_g^{ej}	Fe^{gw}	O^{gw}	Fe^{sw}	O^{sw}	Fe_T	O_T	y_{Fe}	y_O	O_T/Fe_T
3	6.94(11)	1.86(9)	1.24(10)	6.02(9)	1.07(10)	7.88(9)	2.31(10)	0.005	0.019	2.9
1	1.66(11)	5.84(8)	2.10(9)	3.24(9)	3.52(9)	3.82(9)	5.60(10)	0.009	0.013	1.5
0.1	1.35(10)	2.73(7)	6.15(7)	3.21(8)	2.34(8)	3.48(8)	2.91(8)	0.008	0.010	0.8
0.01	1.00(9)	1.14(6)	8.03(5)	2.56(7)	9.25(6)	2.66(7)	1.00(7)	0.008	0.009	0.4
0.001	7.60(7)	3.95(4)	1.65(4)	2.10(6)	4.35(5)	2.14(6)	2.15(6)	0.005	0.0005	0.1

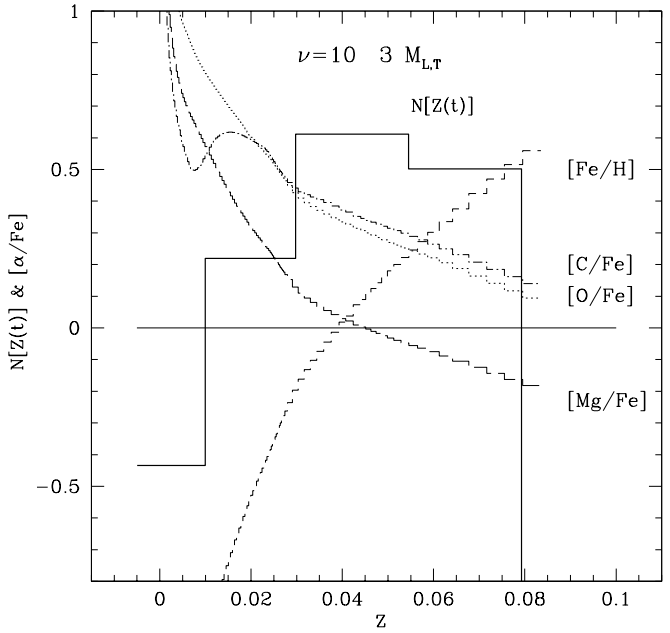

Fig. 12. The relative number distribution of living stars $N[Z(t)]$ per metallicity bin (solid line). $N[Z(t)]$ is on logarithmic scale and in arbitrary units. The relationship between [Fe/H], [C/Fe], [O/Fe], /Fe], and the total metallicity Z. The galaxy on display is the 3 $M_{L,Re}$ model of set A at the age of 15 Gyr. The largest fraction of stars in this galaxy have abundance ratios well above solar. This model is the prototype of a galaxy with enhancement of the α-elements.

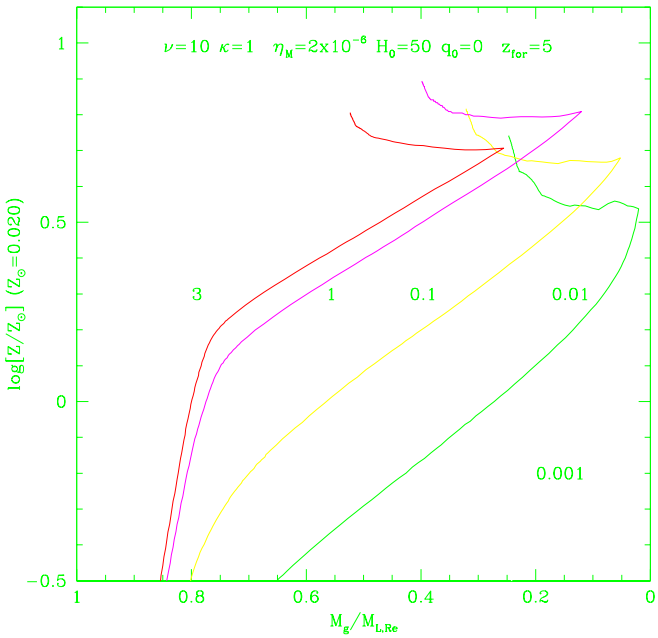

Fig. 13. The relation between the current gas fraction $M_g/M_{L,Re}$ and the current metallicity $Z(t)/Z_\odot$ ($Z_\odot = 0.020$) for all set A models with $\eta_M = 2 \times 10^{-6}$. The minimum value in $M_g/M_{L,Re}$ corresponds to the galactic wind stage. The increase in $M_g/M_{L,Re}$ afterwards is due to dying stars of the previous generations.

the age of 15 Gyr. Similar considerations and conclusions apply to models of the other sets as well. There are two important results out of the data shown in Figs. 11 and 12:

– In the $3M_{L,T}$ galaxy there are very few stars stored in low metallicity bins say up to $Z = 0.01$. This implies that for this galaxy the so-called G-Dwarf analog does not occur. In the opposite extreme, i.e. the $0.001M_{L,T}$ object, about 50% of the stars are in the bins up to $Z = 0.01$, but [Fe/H] increases rapidly to a tenth of solar, so that very few stars of very low Z are found. Also in this case the G-Dwarf analog is avoided. *The kind of IMF we are using naturally secures a lower metallicity cut-off in the distribution of living stars, similar to what required by BCF94 to remove low metallicity stars, and a sort of prompt enrichment in the closed-box model. The need of infall-schemes to avoid the G-Dwarf problem is somehow alleviated by the new IMF.*

– The totality of stars in the $3M_{L,T}$ galaxy have abundance ratios [C/Fe] and [O/Fe] well above solar. As far as the ratio [Mg/Fe] is concerned, it seems that about 50% of stars (those with $Z \leq 0.04$) have the ratio [Mg/Fe] above solar whereas the remaining stars have [Mg/Fe] below solar. Before drawing any conclusion out of this, it should be kept

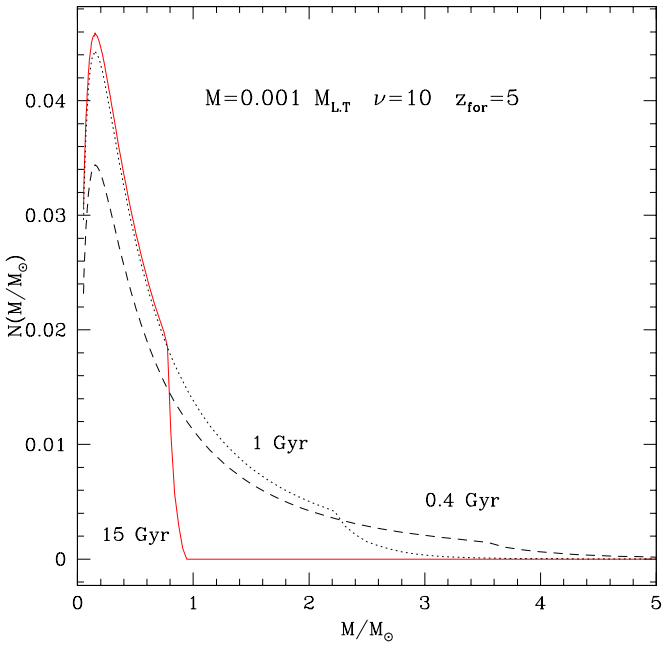

Fig. 14. The theoretical $N(M)$ for the 0.001 $M_{L,T}$ model of set A at three different ages: 0.4 Gyr (solid), 1 Gyr (dotted), and 15 Gyr (dashed).

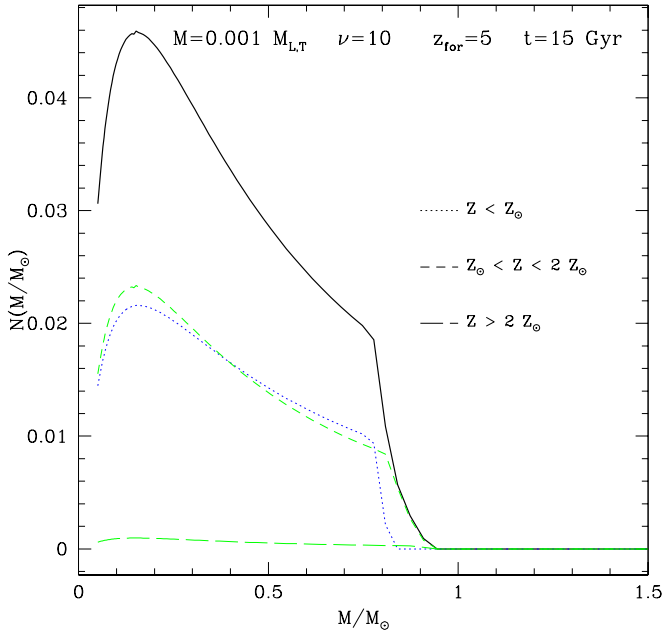

Fig. 15. The theoretical $N(M)$ for the 0.001 $M_{L,T}$ model of set A at the age of 15 Gyr. The top solid line is the total $N(M)$, whereas the other lines are the partial contributions by different metallicity intervals: $Z \leq Z_{\odot}$ (dotted), $Z_{\odot} < Z \leq 2 \times Z_{\odot}$ (dashed), and $Z > 2 \times Z_{\odot}$ (long-dashed).

in mind that the stellar yield of Mg used by Portinari et al. (1998), TCBMP98, and in this paper, underestimates the production of Mg (see Portinari et al. 1998 for all details), so that the Mg abundance cannot be safely used as an indicator of α-enhancement. No difficulty exists with the yield

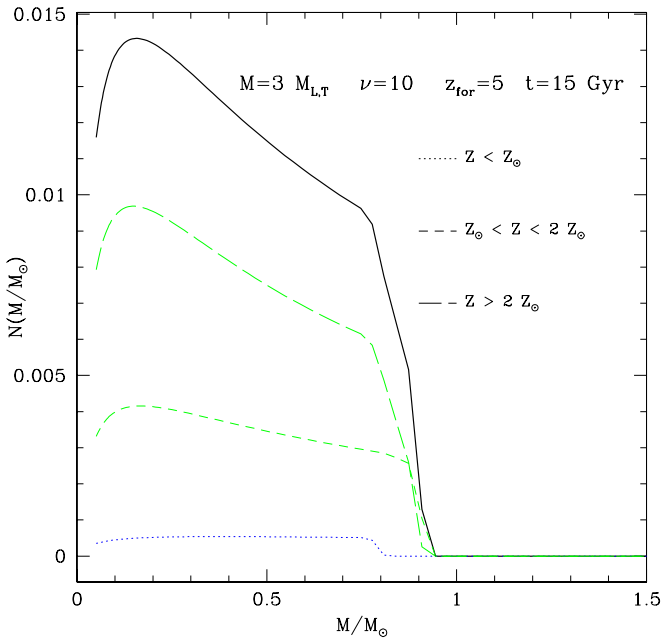

Fig. 16. The theoretical $N(M)$ for the 3 $M_{L,T}$ model of set A at the age of 15 Gyr. The top solid line is the total $N(M)$, whereas the other lines are the partial contributions by different metallicity intervals: $Z \leq Z_{\odot}$ (dotted), $Z_{\odot} < Z \leq 2 \times Z_{\odot}$ (dashed), and $Z > 2 \times Z_{\odot}$ (long-dashed).

of O, whereas there is a marginal discrepancy in the yield of C. Therefore, adopting [O/Fe] as enhancement indicator, we can conclude that this model can be taken as the *prototype of an α-enhanced system*. The opposite occurs with the 0.001 $M_{L,T}$ galaxy in which almost the totality of stars have [O/Fe] and [Mg/Fe] below solar, whereas a large fraction of these (the ones with $Z \geq 0.01$) have [C/Fe] above solar. This model can be taken as the *prototype of a galaxy with no enhancement in α-elements*. Remarkably, this is possible in a system in which the past history of stellar activity although shorter than in the high mass case, still was confined within 0.82 Gyr, too short a time for a significant contamination by Type I supernovae with the classical Salpeter law. The new IMF makes it possible because at the densities typical of the 0.001 $M_{L,T}$ galaxy, the IMF tends to skew toward the low mass end, thus favoring the formation of Type I supernovae.

These results are particularly interesting because two of the most intriguing and at some extend demanding constraints imposed by the observational data, i.e. the G-Dwarf analog and enhancement in α-elements as a function of the galaxy luminosity (mass in turn) are ruled out by the same token.

Finally, in view of the discussion below, we present the relation between the current gas fraction and current metallicity displayed in Fig. 13 (the metallicity is in solar units). The reversal in the trend shown by each curve beyond the minimum value in the gas fraction reached at the wind stage corresponds to the further supply by dying stars. Two notable features can be pointed out: (i) the metallicity is either ever increasing or has a local minimum (effect of the gas restitution by stars of the previous generations); (ii) the fractionary total amount of gas

ejected by dying stars is nearly independent of the galaxy mass, going from 0.28 for the 3 $M_{L,T}$ galaxy to 0.18 for the 0.001 $M_{L,T}$ object (mean value 0.23). Moving from this diagram and the entries of Table 1, one can estimate the total amount of gas and metals made available to the intra-cluster medium by each galaxy. This estimate is a lower limit because we refer only to the R_e-sphere. The amounts of mass in form of oxygen and iron ejected by the galaxies (into the intra-cluster medium) are given in Table 2, whereby the meaning of the symbols is obvious. The data refer only to set A models with $\eta_M = 2 \times 10^{-6}$ for the sake of simplicity. Similar estimates are found for the remaining cases. The contributions at the stage of galactic wind and all over the subsequent history are shown separately. Remarkably, the contribution from the post wind phase parallels or even overwhelms that from the wind stage. The galactic yield ($y_j = M_j/M_{L,Re}$, j stands for the generic element), of Fe varies from $y_{Fe} \simeq 0.005$ to 0.008, depending on the galaxy mass, whereas that for oxygen increases from $y_O \simeq 0.0005$ for the 0.001 $M_{L,T}$ galaxy to 0.018 for the 3 $M_{L,T}$ object. How do these results compare with those by Gibson & Matteucci (1997), who presented similar calculations? Looking at the two model galaxies in common, namely the 1 and 0.001 $M_{L,T}$ objects, and keeping in mind that our models refer to the R_e-sphere (therefore the amounts of ejecta are under-estimated) whereas those by Gibson & Matteucci (1997) are for the whole galaxy, we get the following results (GM and CBPT stand for Gibson & Matteucci and the present paper, respectively):

- 1 $M_{L,T}$: $(\mathrm{GM/CBPT})_{\mathrm{g}} = 2.2$, $(\mathrm{GM/CBPT})_{\mathrm{O}} = 0.3$ and $(\mathrm{GM/CBPT})_{\mathrm{Fe}} = 0.4$ compared to their *standard case*, and $(\mathrm{GM/CBPT})_{\mathrm{g}} = 3.8$, $(\mathrm{GM/CBPT})_{\mathrm{O}} = 0.3$ and $(\mathrm{GM/CBPT})_{\mathrm{Fe}} = 0.4$ compared to their *reduced binding energy model*.
- 0.001 $M_{L,T}$: $(\mathrm{GM/CBPT})_{\mathrm{g}} = 10$, $(\mathrm{GM/CBPT})_{\mathrm{O}} = 10$ and $(\mathrm{GM/CBPT})_{\mathrm{Fe}} = 1$ compared to their *standard case*, and $(\mathrm{GM/CBPT})_{\mathrm{g}} = 13$, $(\mathrm{GM/CBPT})_{\mathrm{O}} = 0.9$ and $(\mathrm{GM/CBPT})_{\mathrm{Fe}} = 0.1$ compared to their *reduced binding energy model*.

We will come back to this topic in the final discussion.

8.4. How does this IMF vary from galaxy to galaxy ?

Owing to the systematic change of the IMF with the physical conditions of the interstellar medium in which stars are formed, we expect the distribution of stars per mass interval $N(M)$ to vary with time and hence metallicity and from galaxy to galaxy. Fig. 14 shows $N(M)$ at three different values of the age, namely 0.2, 0.6, and 15.0 Gyr, for the $0.001M_{L,T}$ galaxy of set A. The drop-off along the three curves at certain values of the mass corresponds to the current value of the turn-off, i.e. 0.98 $M_\odot$ at 15 Gyr, 2.25 $M_\odot$ at 0.6 Gyr, and 3.55 $M_\odot$ at 0.2 Gyr. Notice how at increasing age the part of the $N(M)$ below the turn-off gradually steepens. At the age of 15 Gyr the IMF much resembles the Salpeter law but for the cut-off below 0.15 $M_\odot$. Figs. 15 and 16 shows the inner structure of the $N(M)$ as a function of the metallicity for the $0.001M_{L,T}$ and $3M_{L,T}$ models of set A, respectively, at the constant age of 15 Gyr. The solid line is the total $N(M)$, whereas the dotted, dashed, and long-dashed lines are the partial $N(M)$ in the metallicity intervals $Z \leq Z_\odot$, $Z_\odot < Z \leq 2 \times Z_\odot$, and $Z > 2 \times Z_\odot$, respectively. Note how the trend is reversed passing from the $0.001M_{L,T}$ galaxy to the $3M_{L,T}$ one. In the former, nearly the totality of stars have metallicities smaller than $2 \times Z_\odot$, in the latter the opposite occurs with the majority of stars in the range $Z > Z_\odot$.

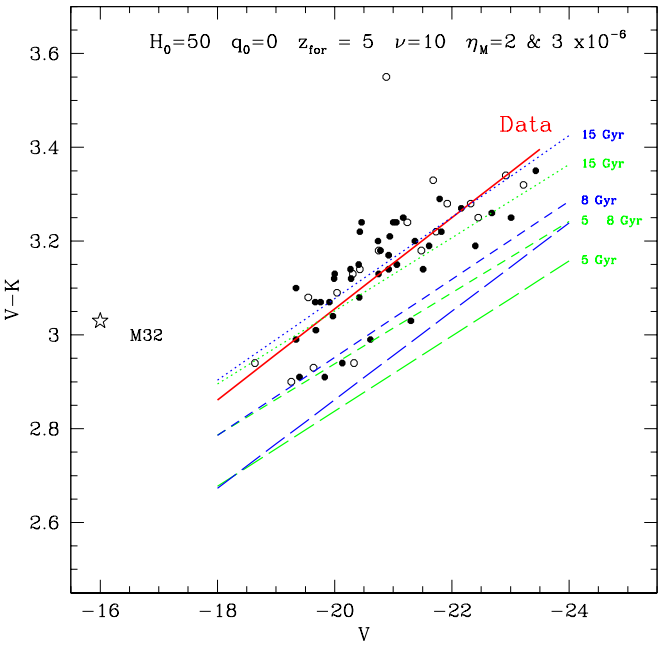

Fig. 17. CMR. The filled and open circles are the data for the Virgo and Coma galaxies of Bower et al. (1992). The distance modulus to Virgo is $(m-M)_0 = 31.54$ (Branch & Tammann 1992), whereas that to Coma is $(m-M)_0 = 35.12$ (Bower et al. 1992). The thick solid line labelled *Data* is the linear square fit of the data. The theoretical relationships are displayed by the linear square fit of the data of Tables 2 and 3 keeping separated the models with different κ and lumping together those with different η. In each pair of lines labelled by the age the bottom line is for $\kappa = 1$ and the top line is for $\kappa = 2$. Three values of the age are considered, namely 15, 8, and 5 Gyr, as indicated.

9. Photometric synthesis: CMR and FP

Since the IMF is no longer constant with respect to time the standard SSP-technique cannot be used to calculate the integrated flux, spectrum, magnitudes, and colors of a galaxy (BCF94, TCBF96). They must be derived from directly calculating the integrated monochromatic flux generated by the stellar content of a galaxy of age T

$$F_\lambda(T) = \int_0^T \int_{M_L}^{M_U} \Psi(t)\phi(t,M) f_\lambda(M,\tau',Z) dt dM \qquad (51)$$

where $f_\lambda(M,\tau',Z)$ is the monochromatic flux of a star of mass M, metallicity $Z(t)$, and age $\tau' = T - t$, and $\Psi(t)$ is the rate of star formation. This poses severe problems of numerical nature and computer storage, of which no details are given here.

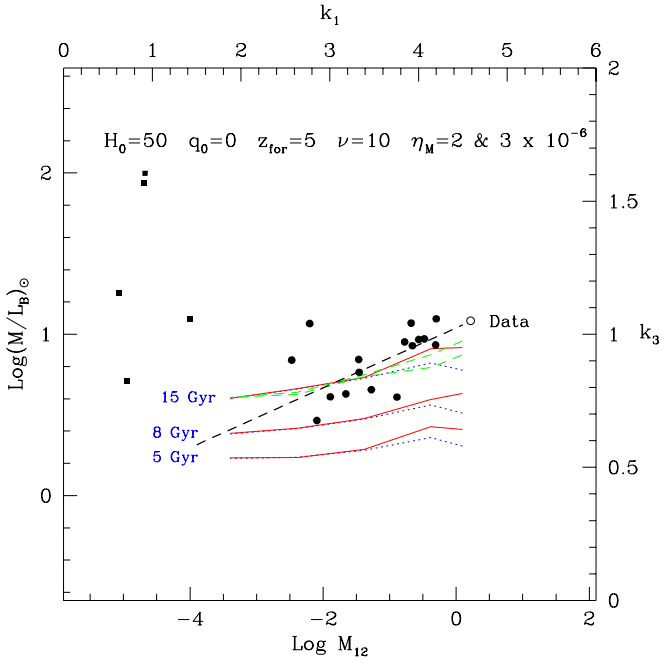

Fig. 18. FP. The theoretical $log(M/L_B)_\odot$ ratios as a function of the total mass $logM_{12}$ for the ages of 15, 8 and 5 Gyr as indicated and models with $\kappa = 1$. The solid lines are for $\eta_M = 3 \times 10^{-6}$, whereas the dotted lines are for $\eta_M = 2 \times 10^{-6}$. In addition, we plot the theoretical relationships for the case with $\kappa = 2$ limited to the age of 15 Gyr (thin dashed lines). The thick dashed line labelled *Data* is the relation for the Virgo galaxies, whereas the filled circles are the data by Bender et al. (1992) for the same objects. The small squares show a few dwarf ellipticals for purposes of comparison.

Finally, the spectral library, the relationship between effective temperature, metallicity, and spectral type of the stars in the various evolutionary stages, in usage here are as in BCF94 and TCBF96 to whom the reader should refer.

The photometric data (magnitudes and colors) in several pass-bands of the Johnson system are listed in Table 3 for all the models (sets A through D) and three values of the age (15, 8 and 5 Gyr). All the magnitudes listed in Table 3 are normalized to the mass $M_{L,Re}$. Real absolute magnitudes are therefore given by

$$M_i = -2.5log(M_{L,Re} \times 10^{12}) + m_i \quad (52)$$

Since our magnitudes M_i refer to the R_e-sphere, they should be converted to total magnitudes before comparing them with the observational data. To a first approximation, one could apply the maximum correction $\Delta M_i = -0.75$ irrespective of the possible of color gradients.

9.1. The color-magnitude relation

The CMR predicted by our models is shown in Fig. 17 for the three values of the age and it is compared to the data of Bower et al. (1992) for the Virgo and Coma galaxies. The adopted distance modulus to Virgo is $(m - M)_0 = 31.54$ (Branch & Tammann 1992), whereas that to Coma is $(m-M)_0 = 35.12$ (Bower et al. 1992). The thick line labelled *Data* is the linear square fit of the observational data. The theoretical CMR are displayed by the linear square fits of the data listed in Tables 3 and 4 separately for models $\kappa = 1$ and $\kappa = 2$ and lumping together the models of the same κ but different η_M. Three values of the age are considered, i.e. 15, 8, and 5 Gyr. Each pair of lines labelled by the age correspond to $\kappa = 1$ (bottom) and $\kappa = 2$ (top). Finally, no correction ΔM_i is applied. Although the agreement with the data is not perfect, yet the slope of the CMR is matched. Indeed the observational data is best compatible with the 15 Gyr relationship of the models with $\kappa = 1$, even though the case $\kappa = 2$ cannot be excluded.

It is worth recalling that even in these models the CMR is a mass-metallicity sequence, because despite the shorter duration of the star forming activity and earlier winds in massive galaxies with respect to the low mass ones, the mean metallicity of the former is higher than in the latter thanks to the compensatory effect of the IMF which skews toward the high mass end. *The great advantage now is that the contradiction between CMR and α-enhancement as far as the overall duration of the star forming activity*
in galaxies of different mass is concerned (cf. Sects. 2.2 and 2.3) does no longer occur.

9.2. Tilt of the fundamental plane

The question to be addressed is: can this IMF account for the slope of the FP without invoking changes in the virial coefficients? To answer this question we have calculated the mass-luminosity ratios $(M/L_B)_\odot$ and $(M/L_K)_\odot$ for all the models of the four sets at three values of the age (5, 8 and 15 Gyr). All the data are listed in Table 4.

The comparison with the observational data for Virgo galaxies is shown in Fig. 18, which displays both the $log(M/L_B)_\odot$ versus $logM_{12}$ plane and the k_3 versus k_1 plane. The filled circles are the data from Bender et al. (1992) and the thick dashed line is the relation $k_3 = 0.15k_1 + 0.36$ presented in Sect. 2.8. For the sake of simplicity first we show the complete case with $\kappa = 1$: the theoretical FP is displayed for three values of the age, namely 15, 8 and 5 Gyr. The solid lines are for $\eta_M = 3 \times 10^{-6}$, whereas the dotted lines are the same but for $\eta_M = 2 \times 10^{-6}$. Limited to the case of 15 Gyr we also show the models with $\kappa = 2$ (thin dashed lines). As expected the difference with respect to the previous case is small and tend to vanish at decreasing galaxy mass. Remarkably, there is no appreciable variation of the slope of the theoretical relation with the age.

Assuming that both the theoretical and the observational FP are represented by linear relationships of the type

$$log(M/L_B)_\odot = A \times logM_{12} + B \quad (53)$$

and

$$k_3 = \alpha \times k_1 + \beta \quad (54)$$

Table 3. Normalized integrated magnitudes m_i of the model galaxies with different ages. Real magnitudes are given by $M_i = -2.5\log(M_{L,R_e} \times 10^{12}) + m_i$. Magnitudes are for the Johnson photometric system. $M_{L,T}$ and M_{L,R_e} are the mass of the galaxy and the mass inside the effective radius, both are in units of $10^{12} M_\odot$; M_s and M_r are the fractionary masses in living stars and collapsed remnants, respectively. The normalization mass is M_{L,R_e}.

$M_{L,T}$	$M_{L,Re}$	Age	M_s	M_r	Mb	U	B	V	R	I	J	H	K
			$\kappa = 1$	$\eta_M = 2 \times 10^{-6}$		$\nu = 10$		$M_l = 0.1 M_\odot$					
3	1.241	15.	0.203	0.140	6.913	9.074	8.587	7.568	6.790	6.129	5.387	4.681	4.487
3	1.241	8.	0.230	0.126	6.277	8.288	7.878	6.901	6.148	5.504	4.775	4.071	3.878
3	1.241	5.	0.253	0.115	5.809	7.682	7.335	6.399	5.668	5.041	4.330	3.631	3.444
1	0.414	15.	0.335	0.204	6.459	8.765	8.205	7.157	6.365	5.682	4.907	4.197	3.997
1	0.414	8.	0.376	0.181	5.836	7.993	7.518	6.513	5.744	5.075	4.304	3.591	3.391
1	0.414	5.	0.411	0.165	5.370	7.387	6.977	6.010	5.264	4.612	3.861	3.152	2.960
0.1	0.041	15.	0.405	0.196	6.230	8.289	7.849	6.852	6.084	5.439	4.723	4.022	3.833
0.1	0.041	8.	0.453	0.170	5.635	7.544	7.176	6.219	5.477	4.851	4.155	3.460	3.272
0.1	0.041	5.	0.491	0.151	5.199	6.970	6.664	5.750	5.031	4.422	3.743	3.054	2.872
0.01	0.004	15.	0.591	0.199	5.875	7.750	7.388	6.427	5.679	5.065	4.408	3.727	3.546
0.01	0.004	8.	0.653	0.165	5.298	7.042	6.739	5.815	5.092	4.497	3.859	3.186	3.006
0.01	0.004	5.	0.701	0.141	4.900	6.500	6.260	5.384	4.686	4.110	3.486	2.822	2.646
0.001	0.0004	15.	0.702	0.141	5.808	7.441	7.169	6.254	5.534	4.965	4.408	3.766	3.601
0.001	0.0004	8.	0.756	0.109	5.286	6.821	6.594	5.711	5.012	4.459	3.908	3.273	3.106
0.001	0.0004	5.	0.798	0.087	4.979	6.349	6.189	5.365	4.698	4.169	3.634	3.016	2.853
			$\kappa = 1$	$\eta_M = 3 \times 10^{-6}$		$\nu = 10$		$M_l = 0.1 M_\odot$					
3	1.241	15.	0.126	0.120	7.466	9.946	9.296	8.216	7.408	6.703	5.891	5.169	4.965
3	1.241	8.	0.143	0.111	6.806	9.086	8.552	7.523	6.742	6.055	5.255	4.532	4.329
3	1.241	5.	0.158	0.104	6.295	8.418	7.958	6.969	6.211	5.543	4.770	4.051	3.857
1	0.414	15.	0.327	0.247	6.474	8.901	8.360	7.352	6.539	5.802	4.927	4.207	3.983
1	0.414	8.	0.368	0.223	5.820	7.949	7.542	6.628	5.852	5.136	4.285	3.567	3.352
1	0.414	5.	0.405	0.205	5.342	7.562	7.085	6.141	5.363	4.628	3.764	3.035	2.825
0.1	0.041	15.	0.398	0.193	6.252	8.331	7.883	6.882	6.112	5.463	4.741	4.038	3.849
0.1	0.041	8.	0.445	0.167	5.657	7.581	7.207	6.247	5.503	4.875	4.174	3.477	3.289
0.1	0.041	5.	0.483	0.149	5.218	7.005	6.692	5.775	5.054	4.443	3.759	3.068	2.885
0.01	0.004	15.	0.590	0.200	5.877	7.761	7.395	6.433	5.684	5.068	4.408	3.725	3.545
0.01	0.004	8.	0.652	0.165	5.297	7.048	6.743	5.817	5.093	4.497	3.857	3.182	3.003
0.01	0.004	5.	0.700	0.141	4.895	6.501	6.259	5.381	4.683	4.105	3.479	2.814	2.638
0.001	0.0004	15.	0.704	0.141	5.810	7.446	7.172	6.258	5.537	4.967	4.410	3.768	3.602
0.001	0.0004	8.	0.757	0.109	5.289	6.826	6.599	5.715	5.016	4.462	3.911	3.276	3.108
0.001	0.0004	5.	0.799	0.087	4.982	6.355	6.194	5.369	4.702	4.173	3.637	3.019	2.855
			$\kappa = 2$	$\eta_M = 2 \times 10^{-6}$		$\nu = 10$		$M_l = 0.1 M_\odot$					
3	1.214	15.	0.369	0.244	6.366	8.680	8.188	7.195	6.395	5.678	4.833	4.119	3.900
3	1.214	8.	0.415	0.218	5.699	7.755	7.376	6.473	5.706	5.004	4.175	3.461	3.249
3	1.214	5.	0.455	0.198	5.226	7.351	6.922	5.995	5.227	4.507	3.663	2.937	2.730
1	0.414	15.	0.248	0.150	6.768	8.971	8.464	7.438	6.656	5.988	5.235	4.524	4.330
1	0.414	8.	0.278	0.134	6.160	8.205	7.780	6.796	6.040	5.390	4.651	3.943	3.749
1	0.414	5.	0.303	0.122	5.700	7.610	7.247	6.302	5.567	4.934	4.214	3.511	3.323
0.1	0.041	15.	0.401	0.192	6.264	8.340	7.893	6.892	6.123	5.475	4.754	4.051	3.861
0.1	0.041	8.	0.448	0.166	5.657	7.584	7.209	6.249	5.505	4.876	4.174	3.476	3.288
0.1	0.041	5.	0.486	0.148	5.205	6.999	6.684	5.765	5.044	4.430	3.743	3.051	2.868
0.01	0.004	15.	0.448	0.161	6.136	7.913	7.589	6.647	5.911	5.315	4.695	4.024	3.851
0.01	0.004	8.	0.496	0.134	5.547	7.201	6.931	6.025	5.312	4.736	4.135	3.473	3.300
0.01	0.004	5.	0.533	0.115	5.153	6.658	6.452	5.597	4.912	4.355	3.768	3.118	2.948
0.001	0.0004	15.	0.660	0.154	5.838	7.510	7.224	6.302	5.578	5.001	4.427	3.776	3.609
0.001	0.0004	8.	0.717	0.121	5.291	6.856	6.618	5.730	5.028	4.468	3.903	3.260	3.092
0.001	0.0004	5.	0.762	0.099	4.938	6.352	6.177	5.343	4.671	4.132	3.579	2.950	2.784
			$\kappa = 2$	$\eta_M = 3 \times 10^{-6}$		$\nu = 10$		$M_l = 0.1 M_\odot$					
3	1.241	15.	0.305	0.234	6.598	9.110	8.547	7.540	6.715	5.955	5.044	4.321	4.090
3	1.241	8.	0.343	0.213	5.921	8.090	7.680	6.785	6.001	5.260	4.373	3.650	3.429
3	1.241	5.	0.377	0.196	5.435	7.770	7.246	6.299	5.504	4.736	3.832	3.094	2.879
1	0.414	15.	0.175	0.140	7.121	9.527	8.918	7.852	7.050	6.355	5.556	4.835	4.633
1	0.414	8.	0.199	0.127	6.479	8.692	8.190	7.174	6.400	5.723	4.940	4.219	4.020
1	0.414	5.	0.218	0.118	5.985	8.047	7.615	6.638	5.886	5.228	4.470	3.754	3.562
0.1	0.041	15.	0.402	0.192	6.270	8.378	7.916	6.910	6.137	5.483	4.753	4.047	3.856
0.1	0.041	8.	0.449	0.166	5.659	7.612	7.226	6.261	5.514	4.880	4.169	3.469	3.280
0.1	0.041	5.	0.487	0.148	5.199	7.020	6.695	5.770	5.045	4.426	3.732	3.036	2.852
0.01	0.004	15.	0.473	0.169	6.091	7.895	7.561	6.614	5.874	5.273	4.642	3.967	3.792
0.01	0.004	8.	0.522	0.141	5.518	7.198	6.919	6.007	5.291	4.709	4.098	3.432	3.257
0.01	0.004	5.	0.560	0.122	5.129	6.663	6.447	5.584	4.895	4.333	3.735	3.081	2.909
0.001	0.0004	15.	0.662	0.155	5.835	7.511	7.223	6.301	5.576	4.999	4.423	3.772	3.604
0.001	0.0004	8.	0.720	0.121	5.288	6.856	6.617	5.728	5.026	4.466	3.899	3.256	3.087
0.001	0.0004	5.	0.764	0.099	4.934	6.351	6.176	5.341	4.668	4.129	3.575	2.945	2.779

Table 4. Integrated magnitudes, colors, and mass to light ratios

$M_{L,T}$	Age	$logM_{L,re}$	$\frac{M_s+M_r}{M_{L,Re}}$	M_{bol}	(B-V)	(V-K)	M_B	M_K	$log(M/L_B)$	$log(M/L_K)$
		$\kappa = 1$	$\eta_M = 2 \times 10^{-6}$	$\nu = 10$	$H_0 = 50$	$q_0 = 0$	$z_{for} = 5$			
3	15	12.09	0.343	-23.32	1.019	3.081	-21.65	-25.75	0.7781	-0.0019
1	15	11.62	0.539	-22.58	1.048	3.160	-20.84	-25.05	0.8216	-0.0016
0.1	15	10.62	0.601	-20.31	0.997	3.019	-18.69	-22.71	0.7265	-0.0199
0.01	15	9.613	0.790	-18.16	0.961	2.881	-16.64	-20.49	0.6608	-0.0159
0.001	15	8.602	0.843	-15.70	0.915	2.653	-14.34	-17.90	0.6014	0.0342
3	8	12.09	0.356	-23.96	0.977	3.023	-22.36	-26.36	0.5106	-0.2294
1	8	11.62	0.557	-23.21	1.005	3.122	-21.52	-25.65	0.5611	-0.2297
0.1	8	10.62	0.623	-20.91	0.957	2.947	-19.37	-23.27	0.4729	-0.2287
0.01	8	9.613	0.818	-18.73	0.924	2.809	-17.29	-21.03	0.4164	-0.2168
0.001	8	8.602	0.865	-16.22	0.883	2.605	-14.91	-18.40	0.3826	-0.1523
3	5	12.09	0.368	-24.43	0.936	2.955	-22.90	-26.79	0.3078	-0.3886
1	5	11.62	0.576	-23.67	0.967	3.050	-22.07	-26.08	0.3592	-0.3876
0.1	5	10.62	0.642	-21.34	0.914	2.878	-19.88	-23.67	0.2811	-0.3757
0.01	5	9.613	0.842	-19.13	0.876	2.738	-17.77	-21.39	0.2373	-0.3483
0.001	5	8.602	0.885	-16.53	0.824	2.512	-15.32	-18.65	0.2305	-0.2439
		$\kappa = 1$	$\eta_M = 3 \times 10^{-6}$	$\nu = 10$	$H_0 = 50$	$q_0 = 0$	$z_{for} = 5$			
3	15	12.09	0.246	-22.77	1.080	3.251	-20.94	-25.27	0.9173	0.0449
1	15	11.62	0.574	-22.57	1.008	3.369	-20.68	-25.06	0.9109	0.0201
0.1	15	10.62	0.591	-20.29	1.001	3.033	-18.66	-22.69	0.7328	-0.0208
0.01	15	9.613	0.790	-18.15	0.962	2.888	-16.64	-20.49	0.6636	-0.0163
0.001	15	8.602	0.845	-15.70	0.914	2.656	-14.33	-17.90	0.6037	0.0356
3	8	12.09	0.254	-23.43	1.029	3.194	-21.68	-25.91	0.6336	-0.1956
1	8	11.62	0.591	-23.22	0.914	3.276	-21.50	-25.69	0.5964	-0.2196
0.1	8	10.62	0.612	-20.89	0.960	2.958	-19.34	-23.25	0.4776	-0.2296
0.01	8	9.613	0.817	-18.73	0.926	2.814	-17.29	-21.03	0.4174	-0.2186
0.001	8	8.602	0.866	-16.22	0.884	2.607	-14.91	-18.40	0.3851	-0.1513
3	5	12.09	0.262	-23.94	0.989	3.112	-22.28	-26.38	0.4095	-0.3709
1	5	11.62	0.610	-23.70	0.944	3.316	-21.96	-26.22	0.4273	-0.4167
0.1	5	10.62	0.632	-21.32	0.917	2.890	-19.85	-23.66	0.2855	-0.3773
0.01	5	9.613	0.841	-19.14	0.878	2.743	-17.77	-21.39	0.2364	-0.3520
0.001	5	8.602	0.886	-16.52	0.825	2.514	-15.31	-18.65	0.2330	-0.2426
		$\kappa = 2$	$\eta_M = 2 \times 10^{-6}$	$\nu = 10$	$H_0 = 50$	$q_0 = 0$	$z_{for} = 5$			
3	15	12.08	0.613	-23.85	0.993	3.295	-22.02	-26.31	0.8707	0.0154
1	15	11.62	0.398	-22.27	1.026	3.108	-20.58	-24.71	0.7935	-0.0001
0.1	15	10.62	0.593	-20.28	1.001	3.031	-18.65	-22.68	0.7383	-0.0145
0.01	15	9.613	0.609	-17.90	0.942	2.796	-16.44	-20.18	0.6282	-0.0069
0.001	15	8.602	0.814	-15.67	0.922	2.693	-14.28	-17.90	0.6082	0.0222
3	8	12.08	0.633	-24.51	0.903	3.224	-22.84	-26.96	0.5598	-0.2310
1	8	11.62	0.412	-22.88	0.984	3.047	-21.26	-25.29	0.5349	-0.2175
0.1	8	10.62	0.614	-20.89	0.960	2.961	-19.33	-23.25	0.4798	-0.2286
0.01	8	9.613	0.630	-18.48	0.906	2.725	-17.10	-20.73	0.3797	-0.2127
0.001	8	8.602	0.838	-16.21	0.888	2.638	-14.89	-18.41	0.3784	-0.1720
3	5	12.08	0.653	-24.99	0.927	3.265	-23.29	-27.48	0.3917	-0.4251
1	5	11.62	0.425	-23.34	0.945	2.979	-21.80	-25.72	0.3352	-0.3744
0.1	5	10.62	0.634	-21.34	0.919	2.897	-19.86	-23.67	0.2837	-0.3827
0.01	5	9.613	0.648	-18.88	0.855	2.649	-17.58	-21.08	0.2004	-0.3412
0.001	5	8.602	0.861	-16.57	0.834	2.559	-15.33	-18.72	0.2138	-0.2834
		$\kappa = 2$	$\eta_M = 3 \times 10^{-6}$	$\nu = 10$	$H_0 = 50$	$q_0 = 0$	$z_{for} = 5$			
3	15	12.09	0.539	-23.64	1.007	3.450	-21.69	-26.14	0.9584	0.0355
1	15	11.62	0.315	-21.92	1.066	3.219	-20.12	-24.41	0.8735	0.0195
0.1	15	10.62	0.594	-20.27	1.006	3.054	-18.63	-22.69	0.7482	-0.0158
0.01	15	9.613	0.642	-17.94	0.947	2.822	-16.47	-20.24	0.6399	-0.0076
0.001	15	8.602	0.817	-15.67	0.922	2.697	-14.28	-17.90	0.6094	0.0218
3	8	12.09	0.556	-24.31	0.895	3.356	-22.55	-26.81	0.6251	-0.2153
1	8	11.62	0.326	-22.56	1.016	3.154	-20.85	-25.02	0.5972	-0.2108
0.1	8	10.62	0.615	-20.88	0.965	2.981	-19.32	-23.26	0.4873	-0.2311
0.01	8	9.613	0.663	-18.51	0.912	2.750	-17.11	-20.77	0.3971	-0.2077
0.001	8	8.602	0.841	-16.22	0.889	2.641	-14.89	-18.42	0.3796	-0.1724
3	5	12.09	0.573	-24.80	0.947	3.420	-22.99	-27.36	0.4646	-0.4222
1	5	11.62	0.336	-23.06	0.977	3.076	-21.43	-25.48	0.3803	-0.3809
0.1	5	10.62	0.635	-21.34	0.925	2.918	-19.85	-23.69	0.2888	-0.3884
0.01	5	9.613	0.682	-18.90	0.863	2.675	-17.58	-21.12	0.2206	-0.3346
0.001	5	8.602	0.863	-16.57	0.835	2.562	-15.33	-18.73	0.2144	-0.2844

and casting the theoretical relation in terms of the observational with one (i.e. α and β) we get

$$log(M/L_B)_\odot = \alpha\sqrt{\frac{3}{2}} \times logM_{12} + \gamma \quad (55) \qquad \gamma = -log(\frac{c_1}{c_2}) + \alpha\sqrt{\frac{3}{2}} \times log(\frac{1}{c_2}) + \sqrt{3} \times \beta. \quad (56)$$

Table 5. Theoretical FP

λ	A	B	$\alpha = A \times \sqrt{\frac{2}{3}}$
B-Band	Age: 15 Gyr	$\kappa = 1$	
2×10^{-6}	0.169 ± 0.028	0.970 ± 0.092	0.138
3×10^{-6}	0.170 ± 0.019	1.020 ± 0.063	0.139
2&3$\times 10^{-6}$	0.170 ± 0.015	0.995 ± 0.049	0.139
B-Band	Age: 15 Gyr	$\kappa = 2$	
2×10^{-6}	0.167 ± 0.023	0.977 ± 0.077	0.136
3×10^{-6}	0.169 ± 0.018	1.018 ± 0.059	0.138
2&3$\times 10^{-6}$	0.171 ± 0.012	1.020 ± 0.039	0.139
K-Band	Age: 15 Gyr	$\kappa = 1$	
2×10^{-6}	0.002 ± 0.004	0.002 ± 0.010	0.001
3×10^{-6}	0.002 ± 0.005	0.015 ± 0.017	0.002
2&3$\times 10^{-6}$	0.002 ± 0.003	0.008 ± 0.010	0.002
K-Band	Age: 15 Gyr	$\kappa = 2$	
2×10^{-6}	0.001 ± 0.003	0.005 ± 0.009	0.001
3×10^{-6}	0.001 ± 0.004	0.013 ± 0.012	0.001
2&3$\times 10^{-6}$	0.002 ± 0.003	0.016 ± 0.010	0.002

Therefore, the theoretical slope A corresponds to the observational one multiplied by the factor $\sqrt{3/2}$, whereas the theoretical zero point contains the observational slope and zero point, and the virial coefficients c_1 and c_2 (see also Burstein et al. 1997).

To compare theory with data we calculate the linear-square fit of $log(M/L_B)_\odot$ and $logM_{12}$ both for $\eta_M = 2 \times 10^{-6}$ and $\eta_M = 3 \times 10^{-6}$ separately, and then for the two cases lumped together to somehow take the uncertainty on this parameter into account. The results are summarized in Table 5 which contains the theoretical slopes and zero points together with their uncertainties, and the corresponding slopes in the $k_3 - k_1$ space. Theoretical and observational slopes find good agreement independently of κ and η (at least for the range of values we have considered). The mean scatter in the zero point is about ± 0.055 which is fully compatible with the observational $\sigma = 0.05$.

What would the results be for η_M either much lower or higher than $2 \div 3 \times 10^{-6}$? We recall here that η_M determines how low in temperature the cooling process can go in a collapsing cloud and fixes M_P, which ultimately drives the efficiency of all the other heating sources. Therefore, the effects of η_M are easy to foresee. If $\eta_M << 2 \div 3 \times 10^{-6}$, M_P falls down to the lower limit of the IMF, which becomes Salpeter-like, not many remnants are left over and the FP flattens out. The effect is more pronounced in the high mass (low density) than low mass (high density) galaxies. The opposite occurs if $\eta_M >> 2 \div 3 \times 10^{-6}$, in which case $log(M/L_B)_\odot$ for massive galaxies gets too high and the FP too steep. The many numerical models computed to check this points show that not only the FP goes wrong but also the CMR (because of the effect of η_M via M_P on the mean metallicity of a galaxy).

In addition to η_M, the CBR limit concurs to set the minimum temperature during the collapse of the star forming clouds in case η_M allows for even lower temperatures.

On the basis of the above considerations, the tilt of the FP and at some extent the CMR as well reflect the thermal history of the star forming gas over the early evolutionary stages and its variation with the galaxy mass. What really matters here is not the parameter η_M *per se*, but what physical mechanism determines the temperature of the gas at the star forming stage. We will came back to this below.

Finally, we have also looked at the $log(M/L_K)_\odot$ ratio as a function of $logM_{12}$: the slope and zero point for the K-passband are given in Table 5. The slope is significantly flatter than in the case of the B-passband.

10. Summary and conclusions

In this paper we have presented the preliminary investigation of the effects of Padoan's et al. (1997) IMF, the shape of which depends on the physical conditions (temperature, density, and velocity dispersion) of the medium in which stars are formed. The main goal of this study was to seek for a picture of galaxy evolution (both chemical and spectro-photometric) in which the pattern of properties of elliptical galaxies can find a coherent explanation. Our major concerns were the CMR, the tilt of the FP, and the enhancement of α-elements in relation to the global duration of the star formation activity, prior to the onset of galactic winds.

The greatest advantages of this IMF with respect to the classical Salpeter law or similar laws in literature, e.g. Scalo (1986 and references therein), Arimoto & Yoshii (1987), Kroupa et al. (1993) are: (i) the slope, function of the mass range; (ii) the natural mass cut-off below which the IMF tends to vanish; (iii) the peak mass M_P that gets very small at decreasing temperature and velocity dispersion, and increasing density of the gas (remarkably, under typical values for these three physical quantities, e.g. those holding for molecular clouds in the solar vicinity, the Salpeter law is recovered); (iv) the departure of the new IMF from the standard ones under different physical conditions, such as those perhaps met in elliptical galaxies of different density and velocity dispersion. This brings a new leverage to the problems under examination.

The new IMF has been applied to models of elliptical galaxies, in which the radial dependence of mass density (both stars and gas) and star formation rate are taken into account. The

present analysis is limited to the region inside R_e. However, the results that one would expect in other (more external) regions of the galaxies are easy to foresee.

The temperature, density, and velocity dispersion governing the IMF have been derived by solving the energy equation in which various sources of heating and cooling are considered, and by adopting a simple-minded model for the thermodynamical description of the gas clouds prone to collapse and the star formation process.

Heating is mainly caused by the radiative cooling of supernova remnants and stellar winds, whereas that by UV radiation from massive stars is found to be marginal as nearly all UV flux is re-processed by dust into the far infrared (Bressan et al. 1998, Granato et al. 1997). However, two more sources of mechanical nature are considered: the first one [H_C] is active only in the very early stages of galaxy formation and evolution and it is meant to take into account that part of the energy liberated by the collapse of the primordial gas that will likely go into heat. It provides a sort of initial condition to start with, or in other words the initial flame of our models. The second one [H_M] is active at all times and somehow takes into account that existing gas clouds will mechanically interact with one another thus causing additional heating. Both sources of heat would require detailed studies that go beyond the scope of this paper. Therefore, both heating rates are affect by a certain degree of uncertainty and H_M, in particular, contains the parameter η_M that has to be chosen in advance and has to be determined by comparing theory with observations.

The temporal evolution of the peak mass over the early evolutionary stages drives the whole problem to which the minimum temperature attainable by collapsing gas clouds, chemical enrichment, cooling, and under suitable circumstances the CBR limit concur. It goes without saying that while the quantitative results are expected to depend on the details of our models and on the their parameters, in particular, the scenario emerging from our analysis does not. The following remarks are worth making:

(1) **History of star formation**. The *overall duration of the star forming activity increases at decreasing galaxy mass (or increasing mean density)*. Specifically, $\Delta t_{SF} \propto M_G^{-1}$ is shorter in massive galaxies and longer in low mass ones. This in spite of the stronger gravitational potential in the former, and as a straight consequence of the varying IMF. The same kind of reasoning applies to different regions of a galaxy: star formation activity lasts longer in the center (high density) than in the external (low density) regions.

(2) **Galactic winds**. The onset of galactic winds occur for the same reasons as in the classical scheme, *however with the opposite trend as far as the galactic mass is concerned*. Early on in massive galaxies, and much later in less massive ones. Despite this, the mean and maximum metallicities increase with the galaxy mass, thus providing the same bottom line for the current interpretation of the CMR as in the classical scenario (a mass metallicity sequence of nearly coeval objects).

(3) **G-Dwarf analog**. The excess of low metallicity stars is easily avoided independently of the galaxy mass, because the relatively top-heavy IMF during the early stages secures prompt enrichment of the gas and a scarce population of low-metallicity stars. This makes the infall scheme somehow superfluous.

(4) **Enhancement of α-elements**. This IMF naturally tends to produce different degrees of enhancement at varying radial distance, age, and galactic mass. At given age and position within a galaxy, the enhancement in α-elements increases with galactic mass. This is the sort of trend expected from the line strength indices in galaxies of different luminosity (mass), cf. Sect. 2.2. At given age and galactic mass, the enhancement in α-elements tends to be stronger going from the center to more external regions, because of the decreasing density favoring more massive stars and in turn shorter durations of the star forming periods. Apparently this trend opposes to what inferred from the gradients in the line strength indices Mg_2 and $\langle \mathrm{Fe} \rangle$ observed in a number of elliptical galaxies (cf. Carollo et al. 1993; Carollo & Danziger 1994a,b). The reality is more complicated than this straight conclusion because the line strength indices do not only correlate with the chemical abundances, but depend also on the age and partition function $N(Z)$, number of stars per metallicity bin (cf. TBC98). It may turn out that a region with prolonged star formation, higher metal content, and lower chemical enhancement (our central regions) may have Mg_2 and $\langle Fe \rangle$ indices stronger than in the more external zones with shorter star forming activity, less metal enrichment, and higher chemical enhancement (cf. TBC98 for all details). Finally, in any case the enhancement in α-elements decreases at increasing age (effect of Type I supernovae).

(5) **Baryonic dark matter**. This IMF tends to favor the formation of remnants (black holes, neutron stars, and white dwarfs, these latter in particular). The percentage of remnants may easily outnumber that of visible stars at least at the present epoch. This holds in massive galaxies in general and/or in low density regions of all galaxies. These stars are obvious candidates to baryonic dark matter, with strong physical and cosmological implications. Is there any observational hint for a large percentage of white dwarfs in the stellar mix of elliptical galaxies ? Bica et al. (1996) analyzing the UV excess in a sample of elliptical galaxies noticed absorption features centered at about 1400 Å and 1600 Å that were common to both strong and weak sources. These absorption features characterize the spectrum of moderately cool white dwarfs (DA5). Easy arguments indicate that in order to reach detectability in the UV, the relative mass fraction of such white dwarfs with respect to the luminous component of the galaxy should be of the order of 10:1.

(6) **Tilt of the FP**. The tilt and tightness of the FP follow from the systematic variation of the IMF with galactic mass and the narrow range permitted to the mean value of T_{knee} that is likely established both by internal and external conditions. The observational FP is best matched by old models (say 15 Gyr) with $\eta_M \simeq 2 \div 3 \times 10^{-6}$ and mean T_{knee} in the range 20 to 40 K. Other values for η_M and T_{knee} in turn would predict FPs either too flat or to steep as compared to the observational data.

How a galaxy manages to get η_M and mean T_{knee} in the above ranges is not clear and perhaps beyond the scope of this paper. In the present models T_{knee} results from internal energy

sources. External sources are not taken into account but for the limit set by the CBR. This latter is mostly effective in low mass galaxies (IMF skewed toward the low mass end) because in the initial stages owing to the scarce energy input from supernovae and stellar wind from massive stars, the temperature will easily reach the limit T_{CBR}. For the purposes of the present study, we have adopted the Friedmann model of the Universe with Hubble constant $H_0 = 50\,\mathrm{km\,s^{-1}\,Mpc^{-1}}$, $q_0 = 0$ and redshift of galaxy formation $z_{for} = 5$ (to which an initial value for $T_{CBR} \simeq 15$ corresponds). Other values for the three parameters are obviously possible. They would anyhow lead to similar results. The effect of increasing z_{for} is straightforward, because at given metallicity (cooling) during the early stages, it would be easier for the collapsing clouds to reach the limit $T_{CBR}[z(t)]$. Needless to say that, increasing z_{for}, higher values of $T_{CBR}[z(t)]$ in the very early stages are implied.

Another possibility is that external conditions, for instance the CBR itself, set the initial gas temperature on the top of which internal processes should be added. This would lead to the interesting possibility that during the early stages T_{knee} correlates with z_{for}. In such a case large variations in T_{knee} over short periods of time are to be expected. However, a thorough exploration of all possible cases is beyond the aims of this paper.

Finally, our analysis of the tilt and tightness of the FP simply proves that a solution is possible without invoking changes in the virial coefficients c_1, and c_2 (see Sect. 2.6) or other effects of dynamical nature (cf. Ciotti et al. 1996). If deviations from virial conditions and/or dynamical effects do actually occur, they will be expected to constitute a minor correction to the gross trend established by the varying IMF.

(7) **On the iron-discrepancy**. Although it is beyond the scope of this paper to address the question of the iron discrepancy raised by the ASCA data, we would like to briefly comment that part of the disagreement could originate from the assignment of the iron abundance to the stellar content of these galaxies. In fact, it partly stems from the adoption of a particular $[\mathrm{Fe/H}]$-$\mathrm{Mg_2}$ calibration, in which no dependence on age and possible enhancement of α-elements is taken into account. We start noticing that the general relationship linking the total metallicity Z to the iron content $[\mathrm{Fe/H}]$ is

$$[\frac{Fe}{H}] = log[\frac{Z}{Z_\odot}] - log[\frac{X}{X_\odot}] + \\ - 0.8 \times [\frac{\alpha}{Fe}] - 0.05 \times [\frac{\alpha}{Fe}]^2 \qquad (57)$$

in which $X_\odot = 0.707$ and $Z_\odot = 0.018$ are the adopted solar values, and the effect of α-elements enhancement is also brought into evidence. This relation reduces to the standard one given by Bertelli et al. (1994) when $[\alpha/\mathrm{Fe}] = 0$ and $X_\odot = 0.700$ and $Z_\odot = 0.020$ are adopted.

Considering that in the course of galactic evolution both helium and heavy elements should have increased according to the popular enrichment law $\Delta Y/\Delta Z = 2 \div 3$ (cf. Pagel et al. 1992), the proper correlation between X and Z of the theoretical SSP and the iron content $[\mathrm{Fe/H}]$ can be established. A recent calibration of the $\mathrm{Mg_2}$ index as a function of the age and metallicity Z (and X) for SSPs is by BCT96 from whom we derive the following analytical approximation

$$[\frac{Fe}{H}] = [7.56 - 0.340 \times t + 0.0148 \times t^2] \times Mg_2 + \\ - [1.325 + 0.0031 \times t + 0.00074 \times t^2] \qquad (58)$$

where t is the age in Gyr, and no effect of α-elements is yet considered. The above relation holds for $0.008 \leq Z \leq 0.05$, $0.20 \leq \mathrm{Mg_2} \leq 0.35$, and ages older than about 5 Gyr, which is fully adequate to our purposes.

For the age of 15 Gyr, this relation is similar to that of Buzzoni et al. (1992) used by Arimoto et al. (1997) in their analysis. Since elliptical galaxies are likely to be rich in α-elements (cf. Sect. 2.2), before assigning $[\mathrm{Fe/H}]$ to the stellar content on the basis of its $\mathrm{Mg_2}$ index, the proper correction for over-abundance by α-elements should be applied, i.e. the value $[\mathrm{Fe/H}]$ read off from Eq. (58) should be decreased by the quantity $-0.8[\alpha/\mathrm{Fe}] - 0.05[\alpha/\mathrm{Fe}]^2$. Considering that $[\alpha/\mathrm{Fe}]$ may vary from 0.5 to 1 according to current data (cf. Matteucci 1997), the expected decrease in $[\mathrm{Fe/H}]$ goes from 3 to 5, which would reduce if not eliminate the disagreement. Looking at the iron over-abundance (with respect to the solar value) versus $log(L_X/L_B)$ diagram of Arimoto et al. (1997), this is the case for NGC 4406, NGC 4636, and NGC 4472 (the galaxies with the highest L_X/L_B ratio). Problems remain with NGC 4374 for which the stellar over-abundance of $\mathrm{Fe/Fe_\odot} = 0.85$ is derived as compared to the value $\mathrm{Fe/Fe_\odot} = 0.11$ indicated by ASCA. Only very high over-abundances of α-elements would be able to remove the discrepancy. That $[\alpha/\mathrm{Fe}]$ can vary from galaxy to galaxy is indicated by extant data. That this applies to NGC 4374 (much higher value in particular) is not granted. Passing we note that the fine structure parameter of this galaxy is 2.3 (Schweizer & Seitzer 1992). The galaxy has suffered from a certain degree of dynamical youth or internal rejuvenation (this is also suggested by its location in $\mathrm{H_\beta}$ versus $[\mathrm{MgFe}]$ plane, cf. BCT96). How this would affect the $\mathrm{Mg_2}$ index is not easily assessable. The problems raised by Arimoto et al. (1997) still persist. In any case, we like to point out that enhancement of α-elements is a natural side product of the new IMF, in particular in the low density regions of a galaxy.

(8) **On the intra-cluster gas**. The data presented in Sect. 8.3 and Table 2 can perhaps alleviate the difficulties encountered by the standard models (cf. Matteucci 1997 for a recent review of the subject) in simultaneously account for amount of iron and gas observed in the ICM. The R_e-sphere of the 1 and 3 $M_{L,T}$ galaxies eject amounts of gas, oxygen, and iron going from 1.6 to $6.9\times10^{11} M_\odot$, 5.6 to $2.3 \times10^{10} M_\odot$ and 3.8 to $7.9 \times10^{9} M_\odot$, respectively. These numbers can be easily doubled considering the contribution from the remaining half of the galaxy not taken into account here. As compared to the estimates by Gibson & Matteucci (1995) for their standard model referred to the whole galaxy, for which they get $\simeq 3.7 \times 10^{11} M_\odot$ of gas, $\simeq 1.6 \times 10^9 M_\odot$ of Fe, and $\simeq 1.7 \times 10^{10} M_\odot$ of oxygen, there is a mean increase by a factor of 1.2 to 2.3 in gas, 2.3 to 4.7 in O, and 3.6 to

7.3 in Fe. Whether this data can completely rule out the above difficulty cannot be said without detailed model calculations convolved with the Schechter (1976) luminosity functions of galaxies. Work is in progress to improve upon the present models and cast light on this topic (Chiosi et al. 1998).

(9) **Going toward complete models**. The models we have presented are limited to the region within the effective radius, and therefore they are not yet able to properly describe complete galaxies nor to make detailed predictions for the amount and the chemical composition of the gas ejected into the ICM. Furthermore, they cannot predict properties specific to the very central regions of galaxies, nor spatial gradients in physical quantities. However, as the leading parameter is density, the results are somehow independent from the particular region for which they have been derived, and may be extended to other regions in other galaxies provided they have the same density. What would the result be going further out in radius, i.e. to regions of lower density ? The answer is obvious and supported by preliminary numerical calculations. More external regions would follow the same trend as passing from a low mass (mean high density) galaxy to a high mass (low mean density) one. The lower density would make it easier to form massive stars and to anticipate the onset of galactic winds. The material expelled from the outer regions of a galaxy should be more enhanced in α-elements and in more generous relative proportions with respect to what is left over as stars. If so, the construction of a galaxy can be viewed as a sort of out-inward process with star formation lasting progressively longer as we move inward.

(10) **Replacing galaxy masses with densities**. All the discussion carried out in so far has been made using the galactic mass as the parameter ranking the various properties instead of the mean density despite the fact that density was the underlying basic parameter. Indeed, the whole discussion could be re-phrased in terms of this latter. This makes the results of our analysis even more general in the sense that they be could applied to sub-units of the same system (proto-galaxy) with different initial mean density of gas. Let us imagine for the sake of argument, that a number of such sub-units can exist within the total potential well of the proto-galaxy (dark and baryonic matter), and start forming stars more or less at the same time in the remote past. A low density cloud will have the peak mass of its IMF skewed toward the high mass end (M_P can easily be higher than what found in our models with the lowest density) and, therefore, will soon experience the conditions for local gas ejection and interruption of star formation. If gas loss is too high, the newly born stellar system may even disgregate dispersing its stars into the global potential well. If not, the stellar aggregate will survive. In any case a scarce population of stars is left over, the vast majority of which will evolve on time scales shorter than the Hubble time becoming compact remnants. All of the other stars (low mass objects) will remain either as a diffuse medium or a low luminosity aggregate within the potential well. In contrast, a high density cloud that preferentially will be located in the center of the potential well, will have the peak mass of its IMF more skewed toward the low mass end, and therefore will continue to form stars for longer periods of time before meeting the conditions for local gas ejection and ceasing star formation. Since high density clouds will lose much less gas than the low density ones, they will survive as formed stellar aggregates eventually merging into a single unit at the center of the galaxy. In the above picture of galaxy formation, the bulk of star formation has taken place in the remote past. How and whether the gas left over by the building process in each sub-unit is thrown into the intergalactic medium cannot be assessed with this simple scheme. Furthermore, the relative number of sub-units and how they eventually coalesce into bigger aggregates is a typical problem to be addressed with the aid of Tree-SPH simulations of galaxy formation and evolution in a given cosmological context (cf. Sect. 1) and goes beyond the aims of the present study.

Acknowledgements. C.C. wishes to thank the Pontificial Academy of Science for its invitation to attend the Vatican Conference on "The Emergence of Structure in the Universe at the Level of Galaxies" (November 25-29, 1996) where a complete report of the results described in this paper was delivered. He is also pleased to acknowledge the hospitality and stimulating environment provided by ESO in Garching where this paper was written up during sabbatical leave from the Astronomy Department of the Padua University. This study has been financially supported by the Italian Ministry of University, Scientific Research and Technology (MURST), the Italian Space Agency (ASI), and the TMR grant ERBFMRX-CT96-0086 from the European Community.

References

Arimoto N., & Yoshii Y., 1987, A&A 173, 23
Arimoto N., & Yoshii Y., 1989, A&A 224, 361
Arimoto N., Matsushita K., Yshimaru Y., Osaki T., & Renzini A., 1997, ApJ, 477, 128
Arnaud M., 1994, in "Clusters of Galaxies", eds. Durret F., Mazure A., Tran Than Van J., Editions Frontieres , Gif-sur-Yvette, p. 211
Arnaud M., Rotheflug R., Boulade O., Vigroux L., & Vangioni-Flam E., 1992, A&A 254, 49
Baugh C.M., Cole S., & Frenk C.S., 1996, MNRAS, in press
Bender R., 1997, in The Nature of Elliptical galaxies, Proceedings of the Second Stromlo Symposium, eds. M. Arnaboldi, G.S. Da Costa & P. Saha, in press
Bender R., Burstein D., & Faber S.M., 1992, ApJ 399, 462
Bertelli G., Bressan A., Chiosi C., Fagotto F., & Nasi E., 1994, A&AS 106, 275
Bertelli G., Bressan A., Chiosi C., Ng Y.K., & Ortolani S., 1995, A&A 301, 381
Bertin G., Saglia R.P., & Stiavelli M., 1992, ApJ 384, 423
Bica E., Bonatto C., Pastoriza M.G., & Alloin D., 1996, A&AS 313, 405
Binney J., & Tremaine S., 1987, *Galactic Dynamics*, Princeton University Press, Princeton, New Jersey
Bower R.G., Lucey J.R., & Ellis R.S., 1992, MNRAS 254, 601
Branch D., & Tammann G.A., 1992, ARA&A, 30 359
Bressan A., Chiosi C., & Fagotto F., 1994, ApJS 94, 63, BCF94
Bressan A., Chiosi C., & Tantalo R., 1996, A&A 311, 425, BCT96
Bressan A., Granato G.L., Silva L., 1998, A&A 332, 135
Bruzual G., & Charlot S., 1993, ApJ 405, 538
Burstein D., Bender R., Faber S.M., & Nolthenius R., 1997, AJ, in press

Burstein D., Bertola F., Buson L.M., Faber S.M., & Lauer T.R., 1988, ApJ 328 440
Buzzoni A. Gariboldi G., & Mantegazza L., 1992, AJ 103, 1814
Caimmi R., & Secco L., 1986, Astrophys. Space Sci. 119, 315
Carollo C. M., & Danziger I.J., 1994a, MNRAS 270, 523
Carollo C. M., & Danziger I.J., 1994b, MNRAS 270, 743
Carollo C.M., Danziger I.J., & Buson L., 1993, MNRAS 265, 553
Carollo C.M., de Zeeuw P.T., van der Marel R.P., Danziger I.J., & Quian E.E., 1995, ApJ 441, L25
Carraro G., Girardi L., Bressan A., & Chiosi C., 1996, A&A 305, 849
Carraro G., Lia C., & Chiosi C., 1998, MNRAS, in press
Charlot S., & Bruzual G., 1991, ApJ 367, 126
Chiosi C., Portinari L., & Tantalo R., 1998, in preparation
Ciotti L., Lanzoni B., & Renzini A., 1996, MNRAS 282, 1
Contardo G., Steinmetz M., Fritze-von Alvensleben U., 1998, ApJ, submitted, (preprint MPA 1076)
David L.P., Forman W., & Jones C., 1991, ApJ 380, 39
Davies R. L., Sadler E. M., & Peletier R.F., 1993, MNRAS 262, 650
Davis M., Efstathiou G., Frenk C.S., & White S.D.M., 1992, Nature 356, 489
Dorman B., O'Connell R.W., & Rood R.T., 1995, A&A 442, 105
Dorman B., Rood R.T., & O'Connell R.W., 1993, A&A 419, 516
Einsel Ch., Fritze-v. Alvensleben U., Krueger H., & Fricke K.J., 1995, A&A 296, 347
Elbaz D., Arnaud M., & Vangioni-Flam E., 1995, A&A 303, 345
Fabbiano G., 1986, PASP 98, 525
Ferguson H.C., & Davidsen A.F., 1993, ApJ 408, 92
Ferguson H.C., Davidsen A.F., Kriss G.A., et al., 1991, ApJ 382, L69
Gibson B.K., 1994, MNRAS 271, L35
Gibson B.K., 1995, Ph.D. Dissertation, University of British Columbia
Gibson B.K., 1996a, ApJ 468, 167
Gibson B.K., 1996b, MNRAS 278, 829
Gibson B.K., 1997, preprint
Gibson B.K., & Matteucci F., 1997, ApJ 475, 47
Gonzáles J.J., 1993, Ph.D. Thesis, Univ. California, Santa Cruz
Granato G.L., Silva L., Danese L., Bressan A., Franceschini A., & Chiosi C., 1997, ESA First Symposium 401
Greggio L., 1996, MNRAS 285, 151
Greggio L., & Renzini A., 1983, A&A 118, 217
Greggio L., & Renzini A., 1990, ApJ 364, 35
Haehnelt M., Steinmetz M., & Rauch M., 1996a, ApJ 465, L95
Haehnelt M., Rauch M., & Steinmetz M., 1996b, MNRAS, 283, 1055
Hollenbach D., 1988, Astro. Lett. and Communications vol. 26, 191
Hollenbach D., & McKee C.F., 1979, ApJS 41, 555
Katz N., 1992, ApJ 391, 502
Katz N., & Gunn J.E., 1991, ApJ 377, 365
Katz N., Weinberg D.H., & Hernquist L., 1996, ApJS 105, 19
Kennicutt, R.C.Jr., 1998, ApJ 498, 541
Kauffmann G., Charlot S., & White S.D.M., 1996, MNRAS 283, L117
Kauffmann G., White S.D.M., & Guiderdoni B., 1993, MNRAS 264, 201
Kodama T., & Arimoto N., 1997, A&A, 320, 41
Kroupa P., Tout C.A., & Gilmore G., 1993, MNRAS 262, 545
Kuntschner H., & Davies R.L., 1998, MNRAS 295, 29
Larson R.B., 1974, MNRAS 166, 585
Larson R.B., 1991, in Frontiers of Stellar Evolution, ed. D.L. Lambert, ASP Conf. Ser. 20, 571
Lee Y-W., 1994, ApJ 423, 248
Longhetti M., Rampazzo R., Bressan A., & Chiosi C., 1997a, A&AS, submitted
Longhetti M., Rampazzo R., Bressan A., & Chiosi C., 1997a, A&AS, submitted
Lynden-Bell D., 1975, Vistas in Astronomy 19, 299
Marigo P., Bressan A., & Chiosi C., 1996, A&A 313, 545
Marigo P., Bressan A., & Chiosi C., 1998, A&A, 331, 564
Matteucci F., 1994, A&A 288, 57
Matteucci F., 1997, Fund. Cosmic Phys. 17, 283
Matteucci F., & Gibson B.K., 1995, A&A 304, 11
Matteucci F., & Greggio L., 1986, A&A 154, 279
Matteucci F., & Vettolani G., 1988, A&A 202, 21
Mushotzsky R., 1994, in Clusters of Galaxies, ed. F. Durret, A. Mazure & Tran Than Van, Gif-sur-Yvette: Editions Frontiers, 167
Navarro J.F., Frenk C.S., & White S.D.M., 1996, ApJ 462, 563
Navarro J.F., & Steinmetz M., 1997, ApJ, 478, 13
Padoan P., Nordlund A.P. & Jones B.J.T., 1997, MNRAS 288, 145
Park J.-H., & Lee Y.-K., 1977, ApJ 476, 28
Pagel B.E.J., Simonson E.A., Terlevich R.J., & Edmunds M.G., 1992, MNRAS, 255, 325
Portinari L., Chiosi C., Marigo P., & Bressan A., 1998, A&A, 334, 505
Renzini A., & Ciotti L., 1993, ApJ 416, L49
Saglia R.P., Bertin G., & Stiavelli M., 1992, ApJ 384, 433
Scalo J.M., 1986, Fund. Cosmic Phys. 11, 1
Scalo J., Vasquez-Semadeni E., Chappell D., Passot T., 1997, ApJ, submitted (astro-ph/9710075)
Schechter P., 1976, ApJ 203, 297
Schmidt M., 1959, ApJ 129, 243
Schombert J.M., Halan P.C., Barsony M., & Rakos K.D., 1993, AJ 106, 923
Schweizer F., & Seitzer P., 1992, AJ 104, 1039
Schweizer F., Seitzer P., Faber S.M., Burstein D., Dalle Ore C.M., & Gonzáles J.J., 1990, ApJ 364, L33
Steinmetz M., 1996a, Proc. Int. School of Physics "Enrico Fermi" - *Dark Matter in the Universe*, Varenna, Italy July 24 - August 4 1995, IOP, Bristol
Steinmetz M., 1996b, MNRAS 278, 1005
Steinmetz M., & Mueller E., 1995, MNRAS 276, 459
Sutherland R.S., & Dopita M.A., 1993 ApJS 88, 253
Talbot R.J., & Arnett D.W., 1973, ApJ 170, 409
Tantalo R., Bressan A., & Chiosi C., 1998b, A&A, in press, TBC98
Tantalo R., Chiosi C., & Bressan A., 1998c, A&A, 333, 419, TCB98
Tantalo R., Chiosi C., Bressan A., & Fagotto F., 1996, A&A 311, 361, TCBF96
Tantalo R., Chiosi C., Bressan A., P. Marigo, & Portinari L., 1998a, A&A 335, 823, TCBMP98
Tegmark M., Silk J. Rees M.J., Blanchard A., Abel T., & Palla F., 1996, ApJ, submitted
Theis Ch., Burkert A., & Hensler G., 1992, A&A 265, 465
Tinsley B.M., 1980, Fundamentals of Cosmic Physics 5, 287
Trentham N., 1994, Nature 372, 157
Young P.J., 1976, AJ 81, 807
Worthey G., 1994, ApJS 95, 107
Worthey G., Faber S.M., Gonzáles J.J., & Burstein D., 1994, ApJS 94, 687